

Material properties and structural behavior of cold-formed steel elliptical hollow section stub columns

Man-Tai Chen ^a, Ben Young ^{b,*}

^{a, b} *Department of Civil Engineering, The University of Hong Kong, Pokfulam Road, Hong Kong, China.*

Abstract

Material properties, residual stress distributions and cross-sectional behavior of cold-formed steel elliptical hollow sections are investigated in this study. Four cross-section series with the nominal section aspect ratio ranging from 1.65 to 3 were included in the experimental investigation. The material properties for each cross-section series and material properties distribution on half of the cross-section profile of a representative section were measured through tensile coupon tests. The distributions of bending and membrane residual stresses in both longitudinal and transverse directions were measured on the half-section profile of the same representative section. Initial local geometric imperfections were measured on five stub column specimens. Besides, stub column tests were conducted between fixed ends to ascertain the material properties of the complete cross-section in the cold-worked state as well as to study the structural behavior of cold-formed steel elliptical hollow section stub columns. In addition to experimental investigation, a finite element model was developed and verified against the test results, with which an extensive parametric study covering a broad range of cross-section geometries was carried out. Currently, there is no codified design rule for elliptical hollow section compression members. The stub column strengths obtained from experimental program and numerical analysis were only compared with the predicted strengths by the equivalent diameter method and equivalent rectangular hollow section approach proposed by previous researchers for design of hot-finished steel elliptical hollow sections, the existing traditional design rules originally developed for circular hollow section with equivalent diameter incorporated as well as the Direct Strength Method and the Continuous Strength Method that the equations were not calibrated for cold-formed steel elliptical hollow sections. The comparisons show that the Direct Strength Method offers the most accurate and reliable design strength predictions among the existing design methods, but further improvement remains possible. In this study, modifications on the Direct Strength Method and the Continuous Strength Method are proposed, which are shown to improve the accuracy of the design strength predictions.

Keywords: Cold-formed steel; Elliptical hollow sections; Residual stresses; Stub columns; Structural design; Tensile coupon tests.

* Corresponding author. Tel.: +852-2859-2674; fax: +852-2559-5337.

E-mail address: young@hku.hk (B. Young).

1. Introduction

Tubular members are frequently used in structural applications, such as buildings, bridges, roof supporting systems and offshore platforms, owing to their superior structural efficiency and aesthetically appealing appearance associated with their closed nature. Cold-forming, as one of the most commonly used steel manufacturing technologies, is a high-speed manufacturing process with quantities of unparalleled merits, such as high-quality surface finish, close repetitive tolerance, high adaptability, easy customization, short manufacturing time and prompt delivery. Recent advances in the cold-forming technology have allowed the derivation of more intricate contours and innovative cross-section shapes by employing different rolling systems. With proper design and arrangement of rolling stations, elliptical hollow section (EHS), being one of the innovative tubular sections, can be easily produced.

Elliptical hollow section integrates the architectural attributes of circular hollow section (CHS) and the structural advantages of rectangular hollow section (RHS). The merits of EHS have drawn attention to researchers and designers. However, previous experimental studies have mainly focused on the behavior of hot-finished steel EHS [1-7] and cold-formed stainless steel EHS [8, 9] with fixed section aspect ratio. Investigation on cold-formed steel EHS is very limited. It was reported by Quach and Young [10] that cold-formed steel EHS behaves quite differently from hot-finished steel EHS in terms of material properties. Different formation methods will lead to the variation of material properties of final steel products and this will surely influence the structural behavior. Therefore, it necessitates the need for this study in order to acquire better understanding on the material properties and structural behavior of cold-formed steel EHS.

This paper describes the investigation on the material properties, residual stress distributions and cross-sectional behavior of cold-formed steel EHS. Tensile coupon tests were conducted on coupon specimens extracted from the critical locations for each cross-section series, namely the flattest and curviest portions, as well as the half-section profile of a representative cross-section to determine the material properties. The distributions of bending and membrane residual stresses in both longitudinal and transverse directions were measured on the half-section profile of the representative section. Prior to stub column tests, initial local geometric imperfections were

measured on each cross-section series. Stub column tests were carried out to ascertain the cross-sectional material properties as well as to study the structural behavior of cold-formed steel EHS in compression. In addition, rigorous finite element (FE) model was developed and validated against the experimental results. Based on the verified FE model of cold-formed steel EHS stub columns, an extensive parametric study covering a broad range of cross-section geometries was performed. It should be noted that there is no codified design rule for cold-formed steel EHS. The experimentally and numerically obtained stub column strengths were compared with the design strengths predicted by the equivalent diameter method [11] and equivalent rectangular hollow section (RHS) approach [12], the existing traditional design rules [13-15] with equivalent diameter as well as the Direct Strength Method (DSM) [13] and the Continuous Strength Method (CSM) [16, 17]. Modifications on the DSM and the CSM are proposed in this study. Reliability analysis was performed to evaluate the reliability of the existing and modified design methods for the design of cold-formed steel EHS stub columns.

2. Experimental investigation

2.1. Test specimens

Four series of EHS were included in the test program. The cross-section geometry of EHS is defined with symbols shown in Fig. 1a. The nominal dimensions ($D \times B \times t$) of EHS are $140 \times 85 \times 3$, $150 \times 50 \times 5$, $150 \times 70 \times 3$ and $180 \times 65 \times 5$, where D , B and t are the overall depth, overall width and wall thickness of the sections, respectively. The nominal section aspect ratio (D/B) of EHS covers a wide range from 1.65 to 3. Series A ($140 \times 85 \times 3$) and Series C ($150 \times 70 \times 3$) were cold-formed from steel plates and then followed by welding, whilst Series B ($150 \times 50 \times 5$) and Series D ($180 \times 65 \times 5$) were cold-formed from hot-extruded seamless steel circular tubes. All EHS are considered as cold-formed steel sections due to the involvement of cold-forming process. The test program consisted of 35 tensile coupon tests, residual stress measurements and 6 stub column tests. The equivalent diameter (D_e) and cross-section classification limit of EHS proposed based on hot-finished steel EHS [2, 6, 18] were adopted for the examination on the range of cross-section slenderness as well as for cross-section classification. The nominal cross-section slenderness of

EHS (D_e/t) in the test program ranged from 77 to 107, and all of which exceed the Class 3 limit of $90\varepsilon^2$ as suggested by previous researchers [2, 6, 18].

2.2. Tensile coupon tests

Tensile coupon tests were conducted to determine the material properties of cold-formed steel EHS at two critical locations for each cross-section series, namely the flattest and curviest portions, as well as half of the cross-section of a representative section ($150\times 70\times 3$). The material properties, including Young's modulus (E), 0.2% tensile proof stress ($\sigma_{0.2}$), ultimate tensile strength (σ_u) and tensile strain at fracture (ε_f), were measured.

2.2.1. Coupon specimens at critical locations

Tensile coupon specimens were machined longitudinally along both the flattest portion (TC1) and the curviest portion (TC2) of each cross-section series of EHS as shown in Fig. 1b. The same tensile coupon dimensions as adopted by Chen and Young [19] for curved coupon specimens were used. Two strain gauges were adhered on both faces in the middle of the gauge length to determine the Young's modulus. The calibrated extensometer with 25 mm gauge length was mounted on the coupon specimen to capture the real-time extension of the specimen within the gauge length and then further converted to the longitudinal strain.

Displacement control with the loading rates of 0.05 mm/min and 0.4 mm/min for elastic and plastic ranges, respectively, was employed to apply the tensile load as recommended by Huang and Young [20] for cold-formed carbon steel. The coupons were tested between two pins installed in a pair of special loading rigs as shown in Fig. 2 so that the coupons were loaded through the centroid of the coupon specimens. All tensile coupon tests were performed using a 50 kN MTS testing machine. The test procedure recommended by Huang and Young [20] was adopted and the tests were paused for 100 seconds at three locations (i.e. near 0.2% proof stress, near the ultimate strength as well as at post-ultimate stage) to allow for stress relaxation and to obtain the static stress-strain relationship. The coupon specimens were tested to fracture and the test is considered to be successful only if the failure occurs within the 25 mm gauge length. The typical stress-strain

histories of coupon specimens at two different critical locations in EHS with nominal dimensions ($D \times B \times t$) of $140 \times 85 \times 3$ are depicted in Fig. 3. The static material properties were obtained and are summarized in Table 1.

For series A and C with nominal cross-section dimensions of $140 \times 85 \times 3$ and $150 \times 70 \times 3$, by comparing the test results of coupon specimens at the flattest and curviest portions, it was found that the strength enhancement due to the cold-forming process is not significant. It is evident by the low level of enhancement of only 0 to 3% and 1 to 6% for 0.2% proof stress and ultimate strength, respectively. The reason for this phenomenon is related to its forming process. Two main manufacturing steps were involved in the cold-forming process, which are from steel coil to circular section and from circular section to the final EHS. In the first step of forming process, when the steel coil was uncoiled and cold-rolled into circular hollow section, there existed more cold-working in the location opposite to the welds compared to the location at a 90° angle from the welds, which corresponds with the locations of the flattest (TC1) and curviest (TC2) portions, respectively. In the second step of forming process, when the circular hollow section was further cold-formed into EHS, it is well accepted that the curviest portion underwent more cold-working than the flattest portion. These two steps of forming process neutralized the strength enhancement at the curviest portion of EHS, and result in a low level of enhancement in 0.2% proof stress and ultimate strength.

For series B and D with nominal cross-section dimensions of $150 \times 50 \times 5$ and $180 \times 65 \times 5$, the coupon specimens at the curviest portions possesses higher 0.2% proof stress and ultimate strength by 28 to 29% and 25 to 37% than the counterparts at the flattest portion, respectively. Significant strength enhancement was observed for these two series of EHS. Unlike the sections in series A and C, in the first step of forming process, the circular hollow sections were formed by hot-extrusion with uniform material properties in the cross-sections. Comparing the test results of coupon specimens at the flattest and curviest portions, the reduction in ductility as represented by the fracture strain of material was quite significant between 35 to 40%.

2.2.2. Coupon specimens in half-section

Coupon tests were conducted on the coupon specimens extracted from half-section of a representative EHS (Series C 150×70×3) to investigate the distribution of material properties in the cross-section. In order to examine the distribution of material properties in a smaller interval, the distance between each coupon specimen was halved and the number of coupon specimens was doubled by extracting the coupon specimens from two successive segments in the same steel tube. The coupon specimens labeled in odd numbers were extracted from one segment and those labeled in even numbers were from a successive segment. The labels and the corresponding locations of coupon specimens are shown in Fig. 4. A total of 27 coupon specimens was tested.

The preparation of coupon specimens as well as test setup and procedure were identical to those described in the previous section of this paper. The material properties obtained from tensile coupon tests in half-section of the representative EHS 150×70×3 are summarized in Table 2. Fig. 4 plots the static material strengths, including 0.2% proof stress and ultimate strength, against the locations of the coupon specimens, which reveals the strength distribution in half-section of the representative EHS. The failed specimens are shown in Fig. 5. From the results, it is obvious that the coupon specimen at the welds possesses the highest 0.2% proof stress and ultimate strength among all coupon specimens in the half of the cross-section. This indicates that the welding material is strong enough to prevent the premature welding failure, which allows the full utilization of the material strength of the section. Excluding the location at the welds, the locations near quarter of EHS had a slightly higher strength than other locations. This may be attributed to the forming process of EHS that local transverse bending was involved at discrete locations such as quarter locations and greater cold-working effect was induced at the corresponding regions.

2.3. Residual stress measurements

For cold-formed steel sections, residual stress is mainly induced by the applied mechanical load from local transverse bending and thermal effect from welding process during manufacturing. It is important to measure and understand the distribution of residual stresses in EHS. The residual

stress distributions were measured on half-section of a representative EHS (150×70×3) in this study.

2.3.1. Method of measurement

There are many techniques in measuring the residual stresses of steel sections, which can be generally categorized into destructive, semi-destructive and non-destructive techniques. The method of sectioning is a commonly adopted destructive technique using the principle of strain release and was adopted in this study.

The total length of specimen was 260 mm, which consisted of a specimen with 250 mm length for longitudinal residual stress measurements and a ring with 10 mm width for transverse residual stress measurements. Strain gauges with 1 mm gauge length were prepared and adhered on both inner and outer surfaces of each 10 mm longitudinal strips as well as the 10 mm ring for longitudinal and transverse stress measurements, respectively. The prepared specimen is shown in Fig. 6. Before cutting, the strain gauges were protected by a waterproofing material to prevent the strain gauges from contaminating by the coolant, which was used to minimize the heat generated during the wire-cutting process.

The initial readings of strain gauges and the room temperature before cutting as well as the readings after cutting were recorded. Five sets of measurements were taken before and after cutting for each strain gauge. The maximum and minimum values among five sets were removed and the average value of the remaining three sets was used in the calculation. The residual strains were calculated based on the differences in strain gauge readings obtained before and after cutting, and were further converted to residual stresses by Hooke's Law. As shown in Fig. 7, residual stresses in the section comprise of the bending and membrane residual stresses (σ_b and σ_m), which can be calculated by Eqs. (1) and (2), respectively. The sign convention of residual stresses and the corresponding deformations are depicted in Fig. 7, which are identical to Chen and Young [18]. The positive and negative values indicate the tensile and compressive residual stresses, respectively.

$$\sigma_b = -E \left(\frac{\varepsilon_o - \varepsilon_i}{2} \right) \quad (1)$$

$$\sigma_m = -E \left(\frac{\varepsilon_o + \varepsilon_i}{2} \right) \quad (2)$$

2.3.2. Longitudinal residual stresses

Residual stresses in longitudinal direction have dominant effect on the structural behavior of sections. To examine the residual stress distributions of a representative EHS (150×70×3), twenty longitudinal strips were sectioned from half of the section. The room temperatures at the time of the measurements before and after cutting were both 20°C. The measured residual strains were converted to residual stresses, which were further normalized to the lowest 0.2% proof stress in the section. The residual stresses and the normalized values were plotted against the location of strip as shown in Figs. 8 and 9, respectively, to show the longitudinal residual stress distributions in half of the cross-section. The results demonstrate that tensile and compressive bending residual stresses were embedded in the section on the outer and inner surfaces, respectively, as evident by the positive values of bending residual stresses for all longitudinal strips. The magnitude of bending residual stress of each strip was higher than the corresponding membrane residual stress. From Figs. 8 and 9, it should be noted that the regions near the quarter locations of the section experienced higher bending residual stress than other regions, which can also be visualized in Fig. 10 by the curvature of the strips after sectioning. The corner, where in the context of this paper corner is the location with maximum curvature, and the quarter locations had localized maximum residual stresses among the adjacent regions. This phenomenon may be attributed to the more cold-working induced by the local transverse bending applied in the forming process at discrete locations such as quarter and corner locations. The distribution of residual stresses was quite symmetric about the curviest portion (corner). The maximum bending residual stress could reach 76.4% of the 0.2% proof stress of the material, while the maximum membrane residual stress was only 27.4% of the 0.2% proof stress of the material.

2.3.3. Transverse residual stresses

In addition to the longitudinal residual stresses, the transverse residual stresses, which refer to the stresses existed in the circumferential direction, were also measured. A total of 14 pairs of strain gauges was attached on the outer and inner surfaces of the 10 mm wide transverse ring. After preparation of the specimen, a cut was applied to the corner with no transverse strain gauge to release the residual stress. The transverse ring opened after cutting and the deformed transverse ring is shown in Fig. 11. The room temperatures at the time of the measurements before and after cutting were both 20°C.

Similar to longitudinal residual stress measurement, the residual stress and the normalized value were plotted against the location of measurement as shown in Figs. 12 and 13, respectively, to show the transverse residual stress distributions in half of the cross-section. The bending residual stresses in most of the region were positive and the membrane residual stresses were all positive, which support the finding that the transverse ring opened after cutting. The distribution of transverse residual stresses was quite symmetric about the curviest portion (corner). The maximum bending and membrane residual stresses reached 86.0% and 18.1% of the 0.2% proof stress of the material, respectively.

2.4. Stub column tests

To determine the material properties and to study the cross-sectional behavior of cold-formed steel EHS in the cold-worked state, six stub columns were tested between fixed ends under uniform axial compression. For the specimen labeling, the first part of the label indicates the nominal cross-section geometry, whilst the second part after the hyphen reveals the specimen type (stub column) and the nominal length of specimen. The symbol # denotes a repeated test. The measured specimen dimensions are reported in Table 3. The nominal length of the stub columns was taken to be 2.5 times the larger outer dimension of the cross-section, except for specimen 180×65×5-SCL270#, which was included for comparison purpose. Before testing, both ends of specimens were milled flat to allow for uniform loading over the cross-section and accurate seating in the testing machine.

2.4.1. Geometric imperfection measurements

Prior to testing, the initial local geometric imperfections for each EHS were measured. The measurement setup and the arrangement of Linear Variable Displacement Transducer (LVDT) as well as the sign convention of local imperfection are depicted in Fig. 14. The specimens were placed on a measurement platform and a LVDT with an accuracy of 0.001 mm was affixed to the head of a milling machine. Owing to the curved surface profile of EHS, one LVDT was used to measure the concavity/convexity along the specimen length at eight different positions, such as the locations with the largest and smallest curvatures as well as the quarter locations, as shown in Fig. 15. Measurements were taken at a 5 mm interval along the specimen length. To eliminate the possible local imperfection induced by cold-sawing of the specimen, measurements were started and terminated 30 mm away from the ends of the specimens. Such procedure was repeated at eight critical locations. The measurements were corrected with reference to the datum taken as a straight line connecting the start and end measurement points. The typical measured local geometric imperfection profile for stub column specimen 150×70×3-SCL375# is shown in Fig. 15. The maximum local geometric imperfections ω_l inherent in the stub column specimens are summarized in Table 3.

2.4.2. Test setup and procedure

To prevent any premature end failure, a pair of special clamping devices with a height of 25 mm was installed near the two ends of specimens with a small gap of around 3 mm between the clamping devices and the adjacent bearing plates. Two pairs of steel inserts were customized made to fit the outer profile of EHS for each stub column specimen and used as the end stiffening special clamping devices. The test setup comprised four LVDTs to measure the end shortening, four strain gauges adhered on the mid-height of specimen at the tips of major and minor axes to determine the axial strain and detect the initiation of local buckling, if any, as shown in Fig. 16. The compressive force was applied to stub column specimens using displacement control at a constant speed of 0.3

mm/min. The applied displacement was paused for 100 seconds near the ultimate load to obtain the static responses of stub column specimens.

2.4.3. Test results

The static stress-strain relationships and load-end shortening responses for all stub columns were obtained as shown in Fig. 17, from which the cross-sectional material properties, ultimate column strengths and the corresponding end shortenings can be further determined as summarized in Tables 4 and 5. Material properties obtained from stub column tests, which were labeled with an additional subscript SC, were compared with those of tensile coupon specimens with the lowest 0.2% proof strength as shown in Table 4. No elastic local buckling was observed during the stub column tests. To further distinguish whether the column failed by cross-section yielding, the squash load (P_y) of the column specimen, which is calculated as the product of the 0.2% proof stresses of material at the flattest portion and the total cross-section area, is compared with the ultimate load-carrying capacity. The specimen was considered to be failed in cross-section yielding when the ratio of ultimate strength to squash load (P_{Exp}/P_y) is greater than unity. From the results as shown in Table 5, all the EHS stub columns in the test program failed by cross-section yielding.

3. Numerical investigation

The finite element model using the program ABAQUS of version 6.14 was developed to simulate the cold-formed steel EHS stub column tests. The finite element model was validated against the test results and further used in extensive parametric study to investigate the cross-sectional behavior of EHS under uniform compression.

3.1. Finite element model

The measured cross-section geometries as reported in Table 3 and the measured Young's modulus were used. The tested engineering stress-strain relationship obtained from the coupon tests at critical locations were converted into the true plastic stress-strain response and were input for the material model.

The fixed-ended boundary conditions of stub columns were simulated by coupling the displacements of the cross-section edges at both ends to the displacements of the corresponding reference points located at the centroid of each cross-section edge. The reference points were restrained against all degrees of freedom, except for the longitudinal displacement at the loading point. The compressive load was applied by specifying the axial displacement of the reference point corresponding to the loading end using a static RIKS step. The nonlinear geometric parameter (*NLGEOM) was enabled to deal with large displacement analysis.

A four-node shell element with reduced integration (S4R) was selected in this investigation, which has been commonly used in modeling the structural members made of metallic material under various types of loading. The sensitivity study on mesh size was conducted to select the proper value of mesh size such that accurate results can be yielded and computation efficiency can also be remained. A uniform mesh of size taken as the minimum of 20 mm and $B/20+(D-B)/10\pi$ along the circumferential and longitudinal directions of the specimens was assigned to the stub column model.

The residual stresses were introduced to the section during the cold-rolling and welding processes. The residual stresses existed in longitudinal direction usually have more influence on the behavior of the structural steel members. The maximum bending and membrane residual stresses are 76.4% and 27.4% of the 0.2% proof stress of the material. Although the embedded bending residual stress in longitudinal direction has a significant magnitude of 76.4% of 0.2% proof stress, the bending residual stress in longitudinal direction is inherently incorporated into the measured material properties from coupon tests. The measured membrane residual stress distribution for series C of EHS was incorporated explicitly in the FE model to investigate whether it is necessary to include the membrane residual stress in the model. Fig. 18 shows the comparison of load-end shortening responses obtained from the stub column models with and without the inclusion of membrane residual stress. The comparison result clearly indicates that the influence of residual stress on the structural response of cold-formed steel EHS is negligible. For simplification, no explicit inclusion of bending and membrane residual stresses in the finite element model is required.

The selection of appropriate buckling mode shape of EHS is important to simulate the buckling behavior of EHS structural members [21, 22]. In this study, the lowest elastic local buckling mode shape obtained by eigenvalue analysis was taken as the initial local geometric imperfection profile of the stub column, and the buckling mode shape was amplified by a certain magnitude of imperfection. Although the measured average value of initial local imperfection for EHS was around $t/3$, the magnitude of imperfection incorporated in the model was determined through sensitivity analysis. Four imperfection amplitudes, expressed as the fractions of section thickness ($t/3$, $t/10$, $t/50$ and $t/100$), were included in the sensitivity analysis, as shown in Table 6, to determine the proper magnitude of the local imperfection to be adopted in the model validation and further parametric study. The magnitude of local imperfection was taken to be $t/50$ in the modeling, which was shown to provide better replication to stub column tests as evident by the mean value of test-to-FE strength ratio close to unity and the possession of small value of coefficient of variation (COV).

3.2. Consideration of strength enhancement of EHS in the FE model

In general, the material strength at the curviest portion was enhanced during the cold-forming process of the EHS as compared to the strength at the flattest portion. The cold-forming effect should also be considered in the modeling process. The strength enhancement was not restricted to the curviest portion where the coupon specimen was extracted and it was extended to a certain region. The sensitivity analysis on the material properties distribution of EHS was conducted. The strength enhancement of EHS at the curviest portion was extended from the tip of the section to a certain distance of the fractions of the larger dimension of the median-profile of the section ($D_m/3$, $D_m/4$, $D_m/6$ and $D_m/10$) as shown in Fig. 19. Table 6 shows sensitivity study results based on different extents of strength enhancement. It is shown that by considering the strength enhancement of the cold-formed steel EHS through extending the material properties at the curviest portion from the tip of the section to $1/6$ of the cross-section depth provides accurate replications for the stub column test strengths. This value of strength enhancement was used in the model validation and parametric study.

3.3. Model validation and parametric study

Based on the aforementioned modeling parameters and assumptions, the finite element model was developed and validated against the EHS stub column tests. The second last column of Table 6 shows the validation results for the FE model used in the parametric study. The FE model can successfully replicate the axial load-carrying capacities of the cold-formed steel EHS stub columns as evident by the mean value and COV of the test-to-FE strength ratio being 0.99 and 0.053, respectively. The comparison of load-end shortening responses obtained from the test and finite element analysis for typical EHS stub column specimen is presented in Fig. 20. The failure mode can also be captured in the finite element model as shown in Fig. 21.

The validated finite element model for stub column was further used to perform extensive parametric study on cold-formed steel EHS under uniform compression. In the parametric study, material properties at the flattest and curviest portions of EHS 140×85×3 were adopted. A total of 56 stub column specimens, which covers extensive range of cross-section dimensions and slenderness, was included in the finite element analysis. The larger dimension of the section (D) varied from 150 to 500 mm. The cross-section aspect ratio (D/B) of the EHS varied from 1.25 to 3.50. Since the expression of cross-section slenderness is not well defined in the current international design specifications [13-15, 23, 24], the equivalent diameter (D_e) defined by Chan *et al.* [11] was adopted to examine the coverage of cross-section slenderness. The cross-section slenderness (D_e/t) defined by Chan *et al.* [11] ranged from 16 to 490 in the parametric study. The length of stub column was taken to be 2.5 times the larger outer dimension of EHS. The results obtained from the numerical study are presented in Table 7.

4. Comparison of stub column strengths with design strengths

No codified design rule is available for cold-formed steel elliptical hollow section compression members. The stub column strengths obtained from experimental program and numerical analysis were compared with the nominal strengths (unfactored design strengths) predicted by the equivalent diameter method [11] and equivalent rectangular hollow section

approach [12] previously proposed for the design of hot-finished steel elliptical hollow sections, the existing traditional design rules [13-15] originally developed for circular hollow section with equivalent diameter incorporated as well as the Direct Strength Method [13] and the Continuous Strength Method [16, 17] that the equations were not calibrated for cold-formed steel elliptical hollow sections.

The material properties obtained from coupon tests in the location with the lowest 0.2% proof stress were used in design calculation for conservative predictions. The existing and modified design methods were examined by reliability analysis as detailed in the North American Specification AISI-S100 [13]. The reliability index (β) is calculated by Eq. (3) based on the statistical parameters as specified in the AISI-S100 [13].

$$\beta = \frac{\ln(M_m F_m P_m C_\phi / \phi)}{\sqrt{V_M^2 + V_F^2 + C_P V_P^2 + V_Q^2}} \quad (3)$$

where $M_m=1.1$ and $F_m=1.0$ are the mean values of material and fabrication factors, $V_M=0.1$, $V_F=0.05$ and $V_Q=0.21$ are the COV of material factor, fabrication factor and load effect, C_P and C_ϕ are correlation and calibration coefficients, ϕ is the resistance factor, P_m and V_P are the mean value and COV of the test-to-predicted strength ratio for different design methods. The load combination of 1.35DL+1.5LL was used in the reliability analysis for the equivalent diameter method and equivalent RHS approach as well as the CSM, whilst load combination of 1.2DL+1.6LL was used for the North American (including the DSM) and American Specifications. For Australian Standard AS4100 [15], the load combination of 1.2DL+1.5LL was adopted in the reliability analysis, where DL and LL mean the dead load and live load, respectively. The values of resistance factor ϕ adopted for different design methods are shown in Table 8. The design method is considered to be reliable only if the reliability index is not less than 2.5.

4.1. Equivalent diameter method proposed by Chan *et al.* [11]

Since no existing design rule is available for the design of elliptical hollow section, Chan *et al.* [11] conducted experimental and numerical investigation on *hot-finished* steel elliptical hollow sections and developed the equivalent diameter method for the cross-section classification and

design strength prediction of hot-finished steel EHS. With the equivalent diameter of EHS under compression expressed by Eq. (4), the cross-section can be classified as slender or non-slender section by adopting the slenderness limit of 90. If the slenderness of EHS ($D_e/t\varepsilon^2$) is larger than 90, the EHS is classified as slender section and the effective area is calculated as per Eq. (5). Subsequently, the nominal stub column strength of EHS (P_{Chan}) is predicted by Eq. (6). The applicability of the equivalent diameter method for the design of *cold-formed* steel elliptical hollow section compressive members was assessed.

The ultimate load-carrying capacities of stub columns obtained from the test and numerical results in this study as well as the tests conducted by Chan *et al.* [25] were compared with the nominal axial strengths predicted by the equivalent diameter method proposed by Chan *et al.* [11] as shown in Fig. 22 and Table 8. In Fig. 22, the test and numerical column strengths to the predicted strengths ratio P_u/P_{Chan} is plotted against the slenderness factor for local buckling (λ_l) as defined in Section 4.6 of this paper. The equivalent diameter method provides very conservative and scattered design strength predictions for cold-formed steel EHS stub columns with the mean value and corresponding COV of P_u/P_{Chan} being 1.53 and 0.263, respectively. The corresponding reliability index is 2.50 for the resistance factor of 1.0, which indicates that the design strength predictions by the equivalent diameter method proposed by Chan *et al.* [11] is marginally reliable.

$$\text{Compression: } D_e = \frac{D^2}{B} \quad (4)$$

$$A_{eff} = A \left[\frac{90}{D_e/t} \frac{235}{f_y} \right]^{0.5} \quad (5)$$

$$P_{Chan} = \begin{cases} Af_y & \text{for } \frac{D_e}{t\varepsilon^2} \leq 90 \\ A_{eff} f_y & \text{for } \frac{D_e}{t\varepsilon^2} > 90 \end{cases} \quad (6)$$

4.2. Equivalent RHS approach proposed by Haque *et al.* [12]

The behavior of EHS lies between that of the circular hollow section (CHS) and rectangular hollow section (RHS). EHS with large aspect ratio had buckling similar to plate buckling in the flat

portions [12]. The equivalent rectangular hollow section approach was proposed by Haque *et al.* [12] for the cross-section classification and design strength prediction of EHS in pure compression. The equivalent RHS maintains the same cross-sectional area as the EHS. For EHS under pure compression, the dimensions of equivalent RHS are expressed by Eq. (7). With the profile of equivalent RHS, each element can be classified based on the new set of slenderness limits proposed by Haque *et al.* [12] and the design strength can be therefore predicted using the principle of effective width method. Since the equivalent RHS approach was developed on the basis of the results of hot-finished steel EHS, the applicability of such approach for the design of *cold-formed* steel EHS compressive members instead of *hot-finished* steel EHS is questionable and was assessed in this study.

The load-carrying capacities of specimens obtained from the test and finite element results in this study as well as the tests conducted by Chan *et al.* [25] were compared with the nominal strengths predicted by the equivalent RHS approach proposed by Haque *et al.* [12] as shown in Table 8 and Fig. 23. The mean value of P_u/P_{Haque} is 1.45 with the corresponding COV of 0.425. The reliability index is 1.72 for the resistance factor of 1.0. The results indicate that the equivalent RHS approach proposed by Haque *et al.* [12] provides quite conservative and scattered as well as unreliable design strength predictions for cold-formed steel EHS stub columns.

$$\text{Compression: } H_e = \frac{A - 2Bt + 4t^2}{2t}; \quad B_e = B \quad (7)$$

4.3. Existing traditional design rules with equivalent diameter

The existing traditional design methods for tubular steel structures [13-15, 23, 24] only cover the structural design of rectangular, square and circular hollow sections, but not elliptical hollow section. The cross-section classification and effective section calculation of cold-formed steel EHS are not specified in any existing traditional design rule. By adopting the equivalent diameter proposed by Chan *et al.* [11], the design rules originally developed for CHS as detailed in various international design specifications [13-15] were used to predict the design strengths of cold-formed steel EHS stub columns. The feasibility of adopting the equivalent diameter proposed by Chan *et*

al. [11] in the Australian Standard AS4100 [15], the North American AISI-S100 [13] and American Specifications ANSI/AISC360 [14] for the design strength predictions of cold-formed steel EHS stub columns was evaluated. The upper limit of slenderness ratio (D_e/t) is specified in different design rules to avoid uneconomic design due to the governance of elastic local buckling for extremely thin tubes. The values of the upper limits of slenderness ratio (D_e/t) are $0.441E/f_y$ and $0.45 E/f_y$ for the North American [13] and American Specifications [14], respectively. The specified upper limit was released in this study to evaluate the applicability of various design rules.

The load-carrying capacities of stub columns obtained from experimental and numerical investigation in this study as well as the tests carried out by Chan *et al.* [25] were compared with the design strengths predicted by the Australian Standard [15], the North American [13] and American Specifications [14] with the equivalent diameter adopted. The comparison results are shown in Table 8 and from Figs. 24 to 26. The mean values of P_u/P_{AS4100}^\dagger , P_u/P_{AISI}^\dagger and P_u/P_{AISC}^\dagger are 5.31, 1.21 and 1.21 with the corresponding COV of 2.240, 0.065 and 0.065 for design strengths predicted by the Australian Standard [15], the North American [13] and American Specifications [14], respectively. The reliability indices are 0.97, 3.53 and 3.29 for the resistance factors of 0.90, 0.85 and 0.90 for the Australian Standard [15], the North American [13] and American Specifications [14], respectively. The results indicate that by employing the equivalent diameter proposed by Chan *et al.* [11], the Australian Standard AS4100 [15] is not capable to predict the design strengths of cold-formed steel EHS stub columns. Whilst the North American [13] and American Specifications [14] provide conservative, but much less scattered design strength predictions for cold-formed steel elliptical hollow section stub columns in a reliable manner.

4.4. Direct Strength Method

Unlike the traditional design approaches, the Direct Strength Method (DSM) as detailed in Chapter E of the AISI-S100 [13] does not require the classification of section. The finite strip method suggested in the DSM is applicable to arbitrary cross-sections for critical elastic buckling stress predictions. Nevertheless, since the DSM design equations were originally calibrated by open sections with plate elements, the applicability and reliability of the DSM for the design strength

predictions of the cold-formed steel EHS stub columns with curved cross-section profile are questionable and therefore, were evaluated in this study.

The nominal axial strength is determined by the minimum of the nominal axial strengths for flexural, torsional or flexural-torsional buckling as well as local buckling and distortional buckling. No distortional buckling and global buckling was observed from the test and numerical studies. The critical elastic column local buckling load was obtained from CUFSM program using the finite strip method [26] with a 1 mm half-wavelength interval. The nominal axial strength can be obtained by substituting the resulted critical elastic local buckling load into the DSM design equations.

The results obtained from experimental and numerical investigation in this study as well as the stub column tests conducted by Chan *et al.* [25] were compared with the DSM predictions as shown in Table 8, Figs. 27 and 28. The mean value of P_u/P_{DSM} is 1.06 with the corresponding COV of 0.093. The reliability index is 2.87 for the resistance factor of 0.85. The results indicate that the existing DSM as detailed in the AISI-S100 [13] provides conservative and reliable design strength predictions for cold-formed steel EHS stub columns. However, further improvement remains possible.

4.5. Continuous Strength Method

The Continuous Strength Method (CSM) is a deformation-based design approach [16, 17] with rational exploitation of the strain hardening of metallic materials and with the consideration of element interaction. Similar to the DSM, the CSM uses full cross-section area instead of effective area and does not involve the cross-section classification. The CSM allows for strain hardening of material by developing the non-linear material models for different metallic materials. Another key component of CSM is the based curve defining the strain capacity for different section types. The material model for cold-formed structural steel section proposed by Buchanan *et al.* [27] was adopted herein for cold-formed steel EHS. The base curve is only available for rectangular hollow section, square hollow section and circular hollow section, but not for the elliptical hollow section as investigated in this study. According to the adopted base curve, there are two approaches in the

Continuous Strength Method, one is the RHS approach for the design of rectangular and square hollow sections and another is the CHS approach for the design of circular hollow section.

The applicability of existing RHS and CHS approaches of the Continuous Strength Method using the corresponding base curves as shown in Eqs. (8) and (9) was assessed. The critical elastic buckling stress of EHS for local buckling involved in the cross-section slenderness (λ_{CSM}) calculation was determined from the finite strip method employed in CUFSM program [26] with a 1 mm half-wavelength interval. The upper limit of cross-section slenderness of 0.6 for CHS approach of the CSM was released in the assessment.

$$\left\{ \begin{aligned} \left(\frac{\varepsilon_{csm}}{\varepsilon_y} \right)_{RHS} &= \frac{0.25}{\lambda_{CSM}^{3.6}} \leq \text{lesser} \left(15, \frac{0.4\varepsilon_u}{\varepsilon_y} \right) && \text{for } \lambda_{CSM} \leq 0.68 \\ \left(\frac{\varepsilon_{csm}}{\varepsilon_y} \right)_{RHS} &= \left(1 - \frac{0.195}{\lambda_{CSM}^{0.8}} \right) \frac{1}{\lambda_{CSM}^{0.8}} && \text{for } \lambda_{CSM} > 0.68 \end{aligned} \right. \quad (8)$$

$$\left\{ \begin{aligned} \left(\frac{\varepsilon_{csm}}{\varepsilon_y} \right)_{CHS} &= \frac{4.44 \times 10^{-3}}{\lambda_{CSM}^{4.5}} \leq \text{lesser} \left(15, \frac{0.4\varepsilon_u}{\varepsilon_y} \right) && \text{for } \lambda_{CSM} \leq 0.3 \\ \left(\frac{\varepsilon_{csm}}{\varepsilon_y} \right)_{CHS} &= \left(1 - \frac{0.224}{\lambda_{CSM}^{0.342}} \right) \frac{1}{\lambda_{CSM}^{0.342}} && \text{for } 0.3 < \lambda_{CSM} \leq 0.6 \end{aligned} \right. \quad (9)$$

The experimental and numerical results obtained from this study as well as the results of stub column tests conducted by Chan *et al.* [25] were compared with the design strength predictions by the RHS and CHS approaches of the CSM as shown in Table 8, Figs. 29 and 30. The mean values of $P_u/P_{CSM,RHS}$ and $P_u/P_{CSM,CHS}$ are 0.98 and 1.09 with the corresponding COV values of 0.068 and 0.045 for design strength predictions by the RHS and CHS approaches of the CSM, respectively. It is found that the RHS and CHS approaches of the CSM provide slightly unconservative and conservative predictions for cold-formed steel EHS stub columns, respectively. The reliability indices are 1.83 and 2.32 for the resistance factor of 1.0, indicating that the design strength predictions by both approaches of existing CSM are not reliable. Modification on the Continuous Strength Method for cold-formed steel EHS stub columns should be carried out.

4.6. Modified Direct Strength Method

The comparison results for the existing DSM reveal that the DSM should be modified for cold-formed steel EHS stub columns to improve the accuracy of design strength predictions. It can be observed from Table 8 that the predictions by existing DSM design equations are slightly scattered compared with the North American [13] and American Specifications [14] predictions. To improve the design predictions for cold-formed steel EHS stub columns, the relationship between P_{nl}^*/P_y and the slenderness factor for local buckling (λ_l) was modified as expressed by Eq. (11). The nominal strengths predicted by the modified DSM (P_{DSM}^*) were equal to P_{nl}^* with consideration of local buckling only since no distortional buckling was observed.

The comparison of test and FE results with the modified DSM design curve is depicted in Table 8, Figs. 28 and 31. The mean value of P_u/P_{DSM}^* is 1.00 with the corresponding COV of 0.044. The accuracy of nominal axial strength prediction was improved by adopting the modified DSM. It is suggested to adopt a more consistent resistance factor of 0.85 for the design of cold-formed steel EHS stub columns for different design methods. The reliability index is 2.82 for the proposed resistance factor of 0.85. The modified DSM provides accurate and the least scattered design strength predictions for cold-formed steel EHS stub columns in a reliable manner.

$$\lambda_l = \sqrt{\frac{P_y}{P_{crl}}} \quad (10)$$

$$P_{nl}^* = \begin{cases} 1.2P_y & \text{for } \lambda_l \leq 0.178 \\ \left[1 - 0.16 \left(\frac{P_{crl}}{P_y} \right)^{0.14} \right] \left(\frac{P_{crl}}{P_y} \right)^{0.14} P_y & \text{for } \lambda_l > 0.178 \end{cases} \quad (11)$$

4.7. Modified Continuous Strength Method

Modified base curve is proposed for EHS as shown in Eq. (12) to modify the CSM in order to cater for the design of EHS. The base curves of RHS and CHS as well as the modified base curve for EHS are shown in Fig. 32. To evaluate the effectiveness of the modified CSM incorporating the modified base curve for EHS, the experimental and numerical results obtained from this study as well as other test results [25] were compared with the design predictions by the modified CSM as

shown in Table 8 and Fig. 33. The mean P_u/P_{CSM}^* is 1.04 and the corresponding COV is 0.059. The reliability index is 2.74 with the proposed resistance factor of 0.85 as consistently adopted in the modified DSM, indicating that the modified CSM is reliable and conservative.

$$\left\{ \begin{array}{l} \left(\frac{\varepsilon_{csm}}{\varepsilon_y} \right)_{EHS} = \frac{0.308}{\lambda_{CSM}^{1.8}} \leq \text{lesser} \left(15, \frac{0.4\varepsilon_u}{\varepsilon_y} \right) \quad \text{for } \lambda_{CSM} \leq 0.52 \\ \left(\frac{\varepsilon_{csm}}{\varepsilon_y} \right)_{EHS} = \left(1 - \frac{0.219}{\lambda_{CSM}^{0.6}} \right) \frac{1}{\lambda_{CSM}^{0.6}} \quad \text{for } \lambda_{CSM} > 0.52 \end{array} \right. \quad (12)$$

5. Conclusions

This paper has presented the investigation on the material properties, residual stress distributions and cross-sectional behavior of cold-formed steel elliptical hollow sections. Material properties and initial local imperfections for each cross-section series were measured. The distributions of material properties and residual stresses on half-section profile of a representative section were determined. Besides, stub column tests were performed to determine the cross-sectional material properties and to study the structural behavior of cold-formed steel elliptical hollow sections. In addition, a numerical model was established and validated against the test results. The strength enhancement of cold-formed steel elliptical hollow section was carefully considered in the finite element model by proposing the extension of material properties at the curviest portion from the tip of the section to a distance of 1/6 of the section depth. A parametric study covering a broad range of cross-section geometries was performed using the validated model. The experimentally and numerically obtained stub column strengths were compared with the design strengths predicted by the equivalent diameter method [11] and equivalent rectangular hollow section approach [12], the existing traditional design rules [13-15] with equivalent diameter as well as the Direct Strength Method [13] and the Continuous Strength Method [16, 17]. The comparisons generally show that the equivalent diameter method, equivalent rectangular hollow section approach and the existing traditional design rules with equivalent diameter incorporated provide very conservative and scattered design strength predictions, whereas the predictions by existing Continuous Strength Method are less scattered and are generally in good agreement with the

experimental and numerical results. The Direct Strength Method predictions are conservative. In this study, modifications on the Direct Strength Method and the Continuous Strength Method are proposed, which are shown to improve the accuracy of the design strength predictions for cold-formed steel elliptical hollow section stub columns in a reliable manner.

Acknowledgements

The authors are grateful to Shenyang Dongyang Special Section Tube for supplying the test specimens. The authors are also thankful to Miss Hoi-Kiu CHAN and Miss Ning-Yan CHAN for their assistance in the experimental program as part of their final year undergraduate research projects at The University of Hong Kong. The research work described in this paper was supported by a grant from the Research Grants Council of the Hong Kong Special Administrative Region, China (Project No. 17267416).

References

- [1] Chan TM, Gardner L. Bending strength of hot-rolled elliptical hollow sections. *Journal of Constructional Steel Research* 2008;64(9):971-986.
- [2] Chan TM, Gardner L. Compressive resistance of hot-rolled elliptical hollow sections. *Engineering Structures* 2008;30(2):522-532.
- [3] Chan TM, Gardner L. Flexural buckling of elliptical hollow section columns. *Journal of structural engineering* 2009;135(5):546-557.
- [4] Law KH, Gardner L. Lateral instability of elliptical hollow section beams. *Engineering Structures* 2012;37:152-166.
- [5] Law KH, Gardner L. Buckling of elliptical hollow section members under combined compression and uniaxial bending. *Journal of Constructional Steel Research* 2013;86:1-16.
- [6] Gardner L, Chan TM. Cross-section classification of elliptical hollow sections. *Steel and Composite Structures* 2007;7(3):185-200.
- [7] Gardner L, Chan TM, Wadee MA. Shear response of elliptical hollow sections. *Structures and Buildings* 2008;161(6):301-309.

- [8] Theofanous M, Chan TM, Gardner L. Structural response of stainless steel oval hollow section compression members. *Engineering Structures* 2009;31(4):922-934.
- [9] Theofanous M, Chan TM, Gardner L. Flexural behaviour of stainless steel oval hollow sections. *Thin-Walled Structures* 2009;47(6):776-787.
- [10] Quach WM, Young B. Material properties of cold-formed and hot-finished elliptical hollow sections. *Advances in Structural Engineering* 2015;18(7):1101-1114.
- [11] Chan TM, Gardner L, Law KH. Structural design of elliptical hollow sections: a review. *Proceedings of the Institution of Civil Engineers-Structures and Buildings* 2010;163(6):391-402.
- [12] Haque T, Packer JA, Zhao XL. Equivalent RHS approach for the design of EHS in axial compression or bending. *Advances in Structural Engineering* 2012;15(1):107-120.
- [13] AISI-S100 2016. North American Specification for the design of cold-formed steel structural members. *AISI S100-16*. Washington, D.C., USA: American Iron and Steel Institute.
- [14] ANSI/AISC360 2016. Specification for Structural Steel Buildings. *ANSI/AISC 360-16*. Chicago, IL, USA: American Institute of Steel Construction.
- [15] AS4100 1998. Steel structures. *AS 4100: 1998*. Homebush, New South Wales, Australia: Standards Australia.
- [16] AISC 2013. Structural Stainless Steel. *AISC Design Guide 30*. American Institute of Steel Construction.
- [17] Gardner L. The continuous strength method. *Structures and Buildings* 2008;161(3):127-133.
- [18] McCann F, Fang C, Gardner L, Silvestre N. Local buckling and ultimate strength of slender elliptical hollow sections in compression. *Engineering Structures* 2016;111:104-118.
- [19] Chen MT, Young B. Cross-sectional behavior of cold-formed steel semi-oval hollow sections. *Engineering Structures* 2018;(Submitted).
- [20] Huang Y, Young B. The art of coupon tests. *Journal of Constructional Steel Research* 2014;96:159-175.
- [21] Silvestre N. Buckling behaviour of elliptical cylindrical shells and tubes under compression. *International Journal of Solids and Structures* 2008;45(16):4427-4447.

- [22]Silvestre N, Gardner L. Elastic local post-buckling of elliptical tubes. *Journal of Constructional Steel Research* 2011;67(3):281-292.
- [23]AS/NZS4600 2005. Cold-formed steel structure. *AS/NZS 4600:2005*. Sydney, Australia: Standards Australia/Standards New Zealand.
- [24]EN1993-1-1 2005. Design of steel structures–Part 1.1: General rules and rules for buildings. *EN 1993-1-1:2005*. Brussels, Belgium: European Committee for Standardization.
- [25]Chan TM, Huai YM, Wang W. Experimental investigation on lightweight concrete-filled cold-formed elliptical hollow section stub columns. *Journal of Constructional Steel Research* 2015;115:434-444.
- [26]Schafer BW, Ádány S. Buckling analysis of cold-formed steel members using CUFSM: conventional and constrained finite strip methods. In: Eighteenth International Specialty Conference on Cold-Formed Steel Structures, Orlando, FL, USA; 2006. p. 39-54.
- [27]Buchanan C, Gardner L, Liew A. The continuous strength method for the design of circular hollow sections. *Journal of Constructional Steel Research* 2016;118:207-216.

Nomenclature

A	Area of the section
A_{eff}	Effective area of the section
B	Overall width of the section
B_e	Width of the equivalent RHS
CHS	Circular hollow section
COV	Coefficient of variation
C_P	Correlation coefficient
CSM	Continuous strength method
C_ϕ	Calibration coefficient
D	Overall depth of the section
D_e	Equivalent diameter
D_m	Larger dimension of the median-profile of the EHS

DSM	Direct strength method
E	Young's modulus
EHS	Elliptical hollow section
E_{SC}	Young's modulus obtained from stub column test
F_m	Mean value of fabrication factor
f_y	Yield stress
H_e	Height of the equivalent RHS
M_m	Mean value of material factor
P_{AISC}^\dagger	Nominal axial strength predicted by American Specification ANSI/AISC360 [14] with equivalent diameter
P_{AISI}^\dagger	Nominal axial strength predicted by North American Specification AISI-S100 [13] with equivalent diameter
P_{AS4100}^\dagger	Nominal axial strength predicted by Australian Standard AS4100 [15] with equivalent diameter
P_{Chan}	Nominal axial strength predicted by the equivalent diameter method proposed by Chan <i>et al.</i> [11]
P_{crl}	Critical elastic local buckling load of member
P_{CSM}^*	Nominal axial strength predicted by the modified Continuous Strength Method
$P_{CSM,CHS}$	Nominal axial strength predicted by the CHS approach in the Continuous Strength Method
$P_{CSM,RHS}$	Nominal axial strength predicted by the RHS approach in the Continuous Strength Method
P_{DSM}	Nominal axial strength predicted by the Direct Strength Method
P_{DSM}^*	Nominal axial strength predicted by the modified Direct Strength Method
P_{Exp}	Experimental loading capacity
P_{FE}	Finite element loading capacity
P_{Haque}	Nominal axial strength predicted by the equivalent RHS approach proposed by Haque <i>et al.</i> [12]

P_m	Mean value of test-to-predicted strength ratio
P_{nl}^*	Nominal axial strength of column for local buckling
P_u	Ultimate axial loading capacity
P_y	Squash load of cross-section
RHS	Rectangular hollow section
t	Thickness of the section
TC	Tensile coupon specimen
V_F	Coefficient of variation of fabrication factor
V_M	Coefficient of variation of material factor
V_P	Coefficient of variation of test-to-predicted strength ratio
V_Q	Coefficient of variation of load effect
β	Reliability index
β^Δ	Reliability index with proposed resistance factor of 0.85
δ_u	End shortening at ultimate load
ε_{csm}	Limiting strain for the cross-section
ε_f	Tensile strain at fracture
ε_i	Residual strain on inner surface
ε_o	Residual strain on outer surface
ε_u	Ultimate strain
ε_y	Yield strain
ϕ	Resistance factor
ϕ^Δ	Proposed resistance factor
λ_{CSM}	Cross-section slenderness in the Continuous Strength Method
λ_l	Slenderness factor for local buckling
σ_b	Bending residual stress
σ_m	Membrane residual stress
σ_u	Static ultimate tensile strength of material
σ_{u-SC}	Static ultimate tensile strength of material obtained from stub column test

σ_{u-TC}	Static ultimate tensile strength of material obtained from tensile coupon test
$\sigma_{0.2}$	Static 0.2% tensile proof stress of material
$\sigma_{0.2-SC}$	Static 0.2% tensile proof stress of material obtained from stub column test
$\sigma_{0.2-TC}$	Static 0.2% tensile proof stress of material obtained from tensile coupon test
ω_l	Initial local geometric imperfection

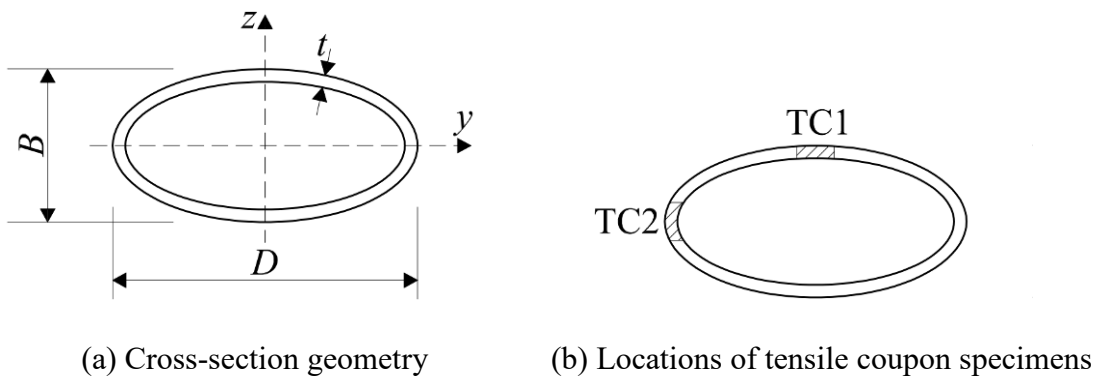


Figure 1. Cross-section of EHS



Figure 2. Setup of coupon tests of EHS

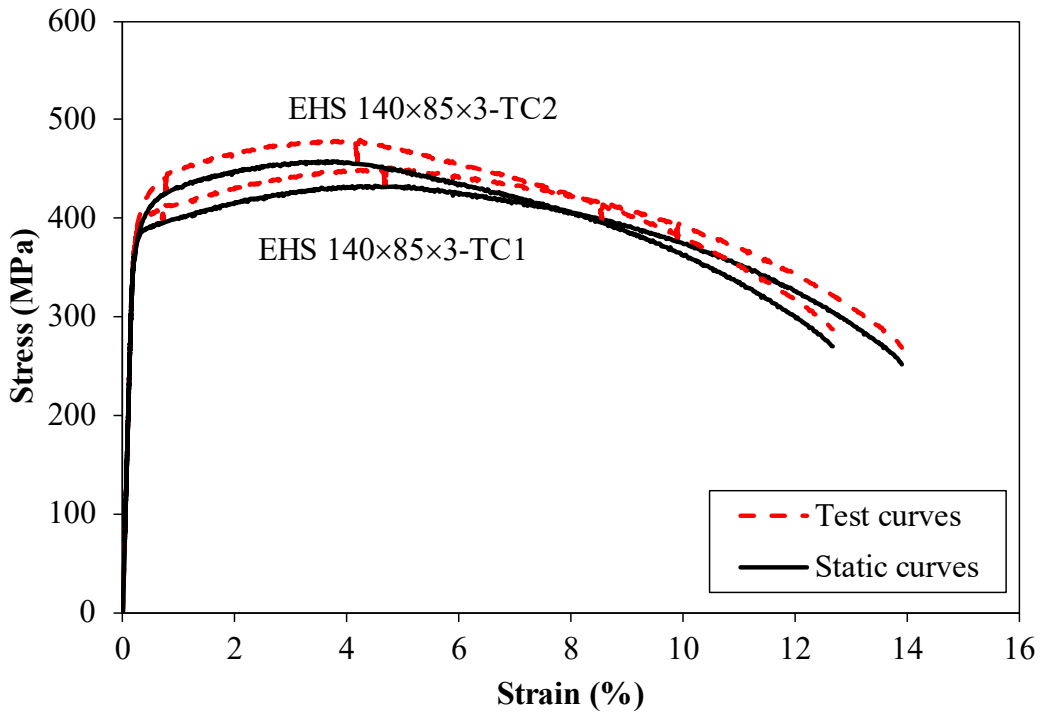


Figure 3. Test and static stress-strain histories of EHS 140×85×3

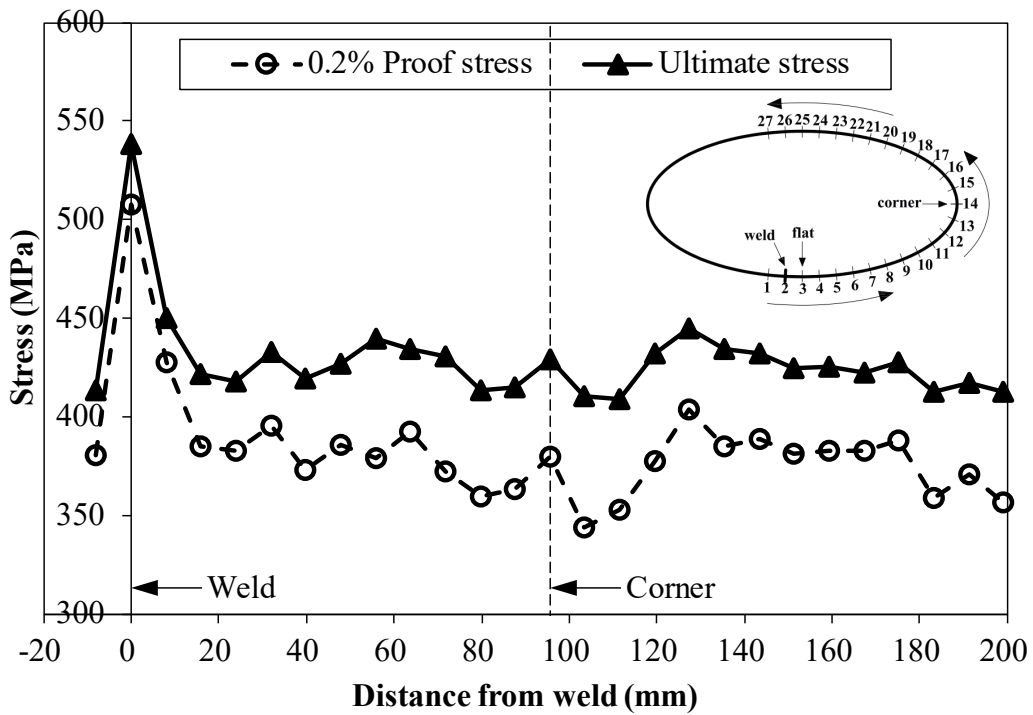


Figure 4. Measured material strengths distribution in EHS 150×70×3



Figure 5. Failed coupon specimens extracted from the half-section of EHS 150×70×3

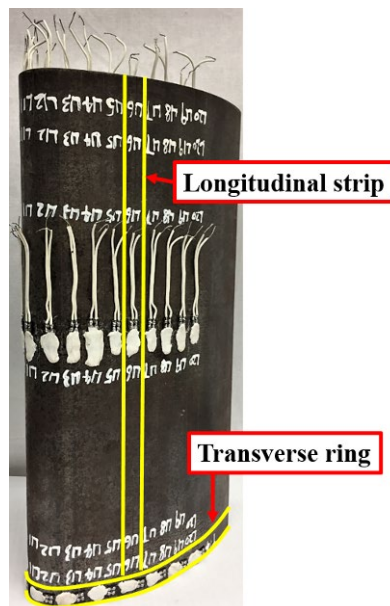


Figure 6. Specimen for residual stress measurements of EHS 150×70×3

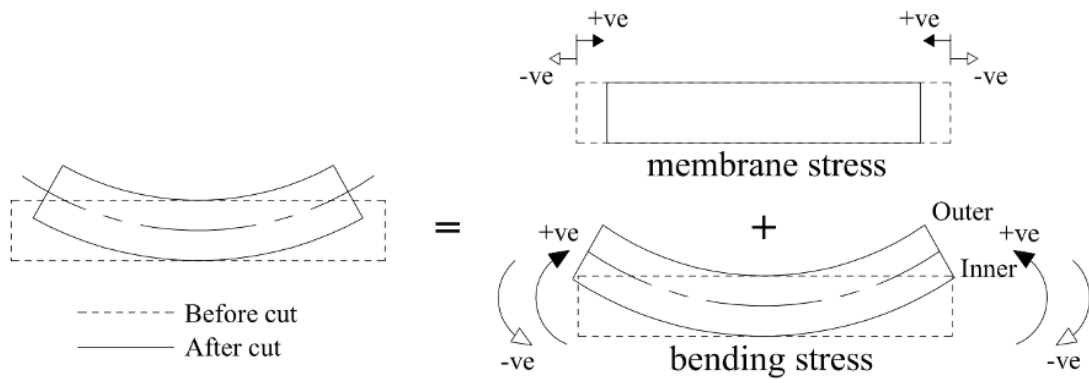


Figure 7. The sign convention for bending and membrane residual stresses [18]

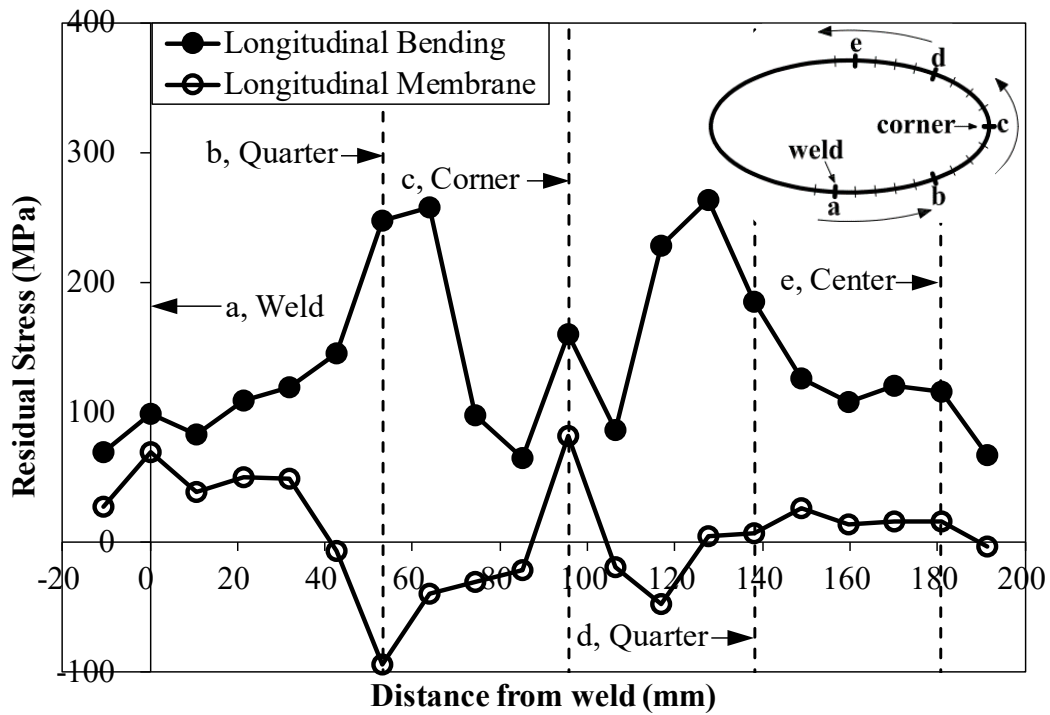


Figure 8. The bending and membrane residual stresses distributions of EHS 150×70×3 in longitudinal direction

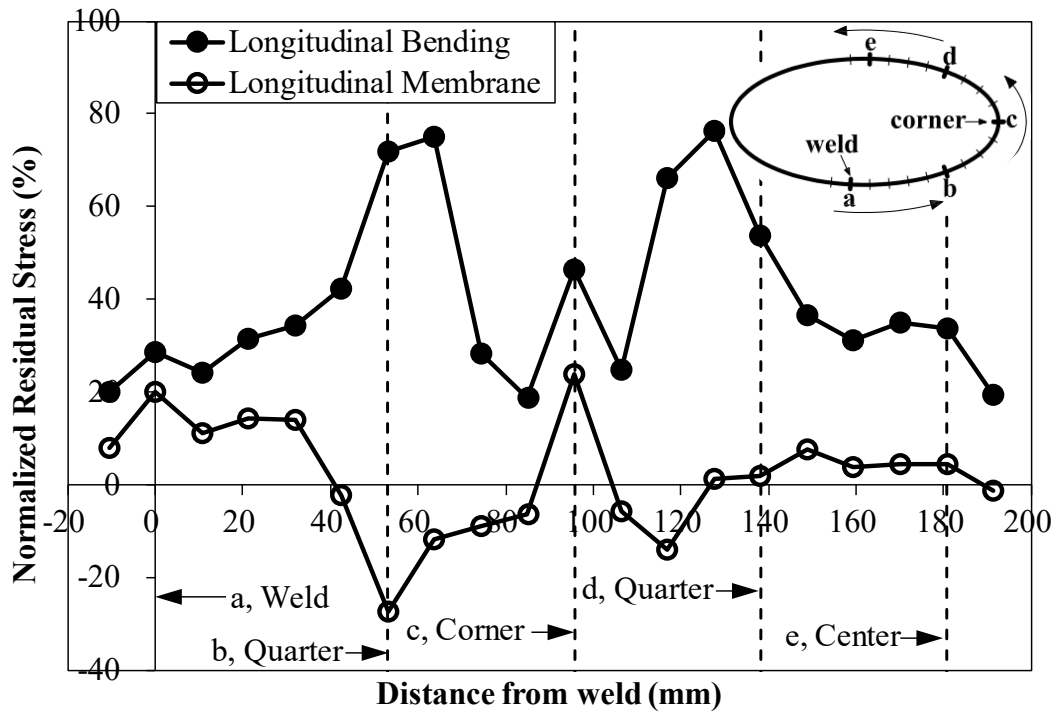


Figure 9. The normalized residual stresses distributions of EHS 150×70×3 in longitudinal direction

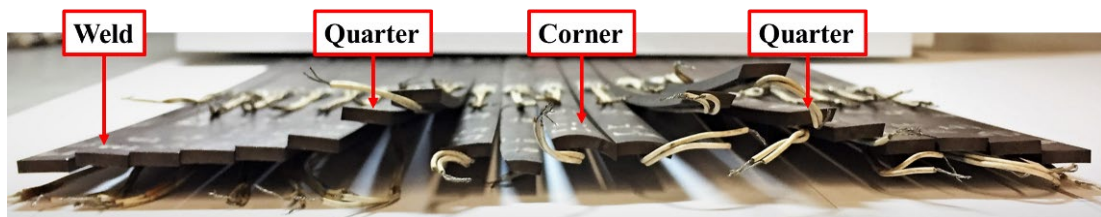


Figure 10. Deformed longitudinal strips of EHS 150×70×3 after cutting



Figure 11. Deformed transverse ring of EHS 150×70×3 after cutting

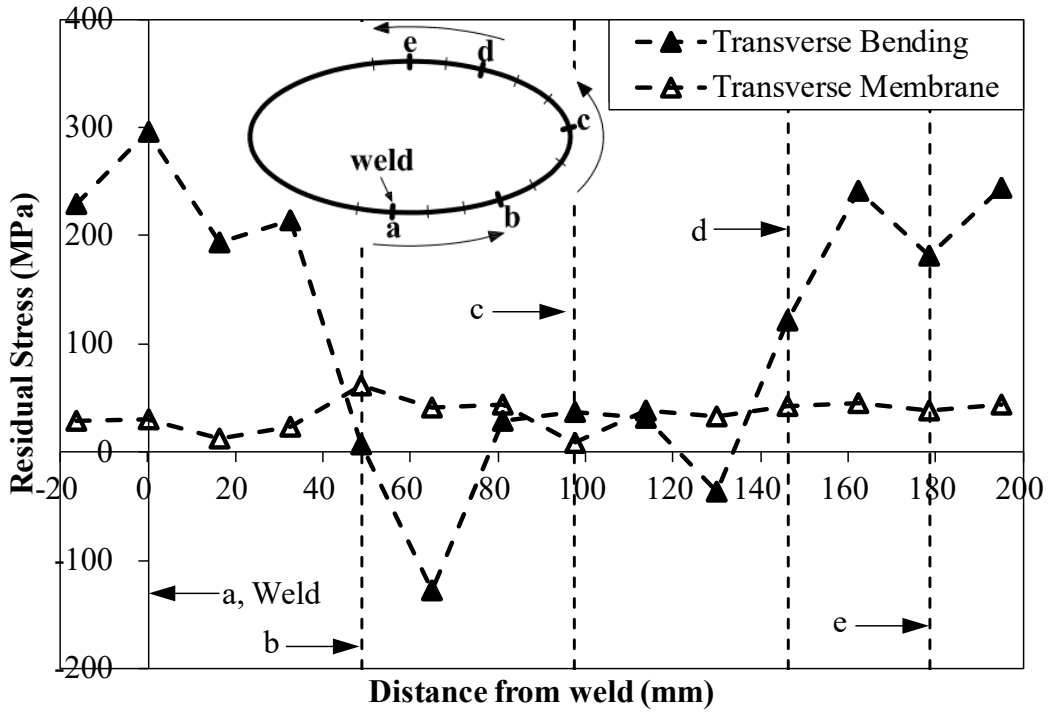


Figure 12. The bending and membrane residual stresses distributions of EHS 150×70×3 in transverse direction

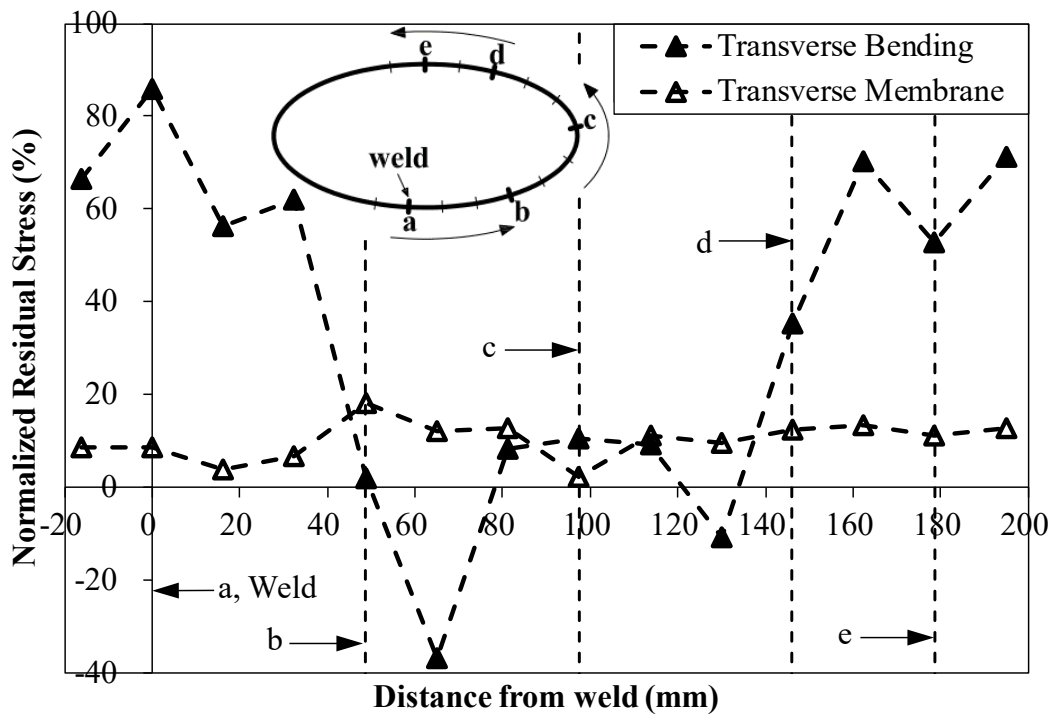
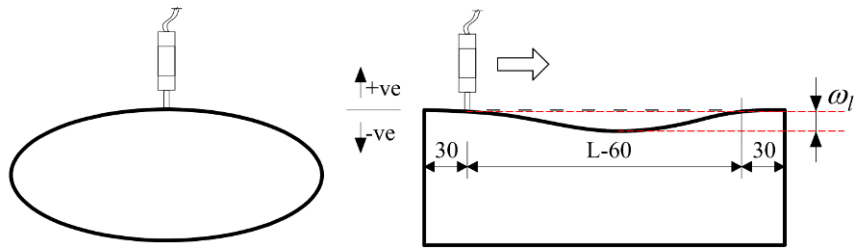


Figure 13. The normalized residual stresses distributions of EHS 150×70×3 in transverse direction



(a) Schematic view



(b) Experimental arrangement

Figure 14. Setup of local geometric imperfection measurements for EHS

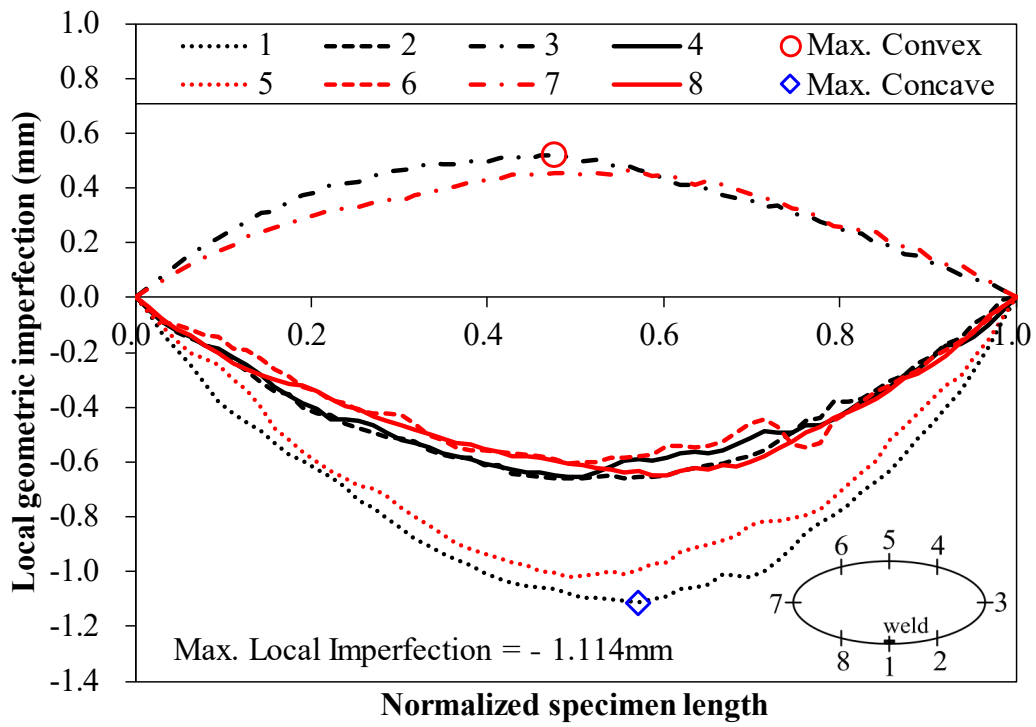
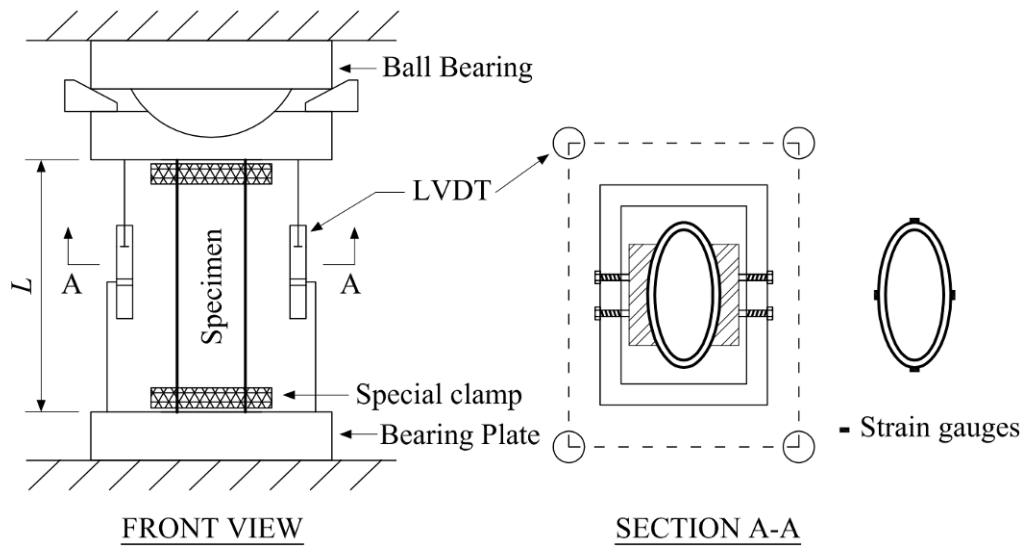


Figure 15. The distributions of local geometric imperfections along the length of EHS stub column specimen 150×70×3-SCL375#

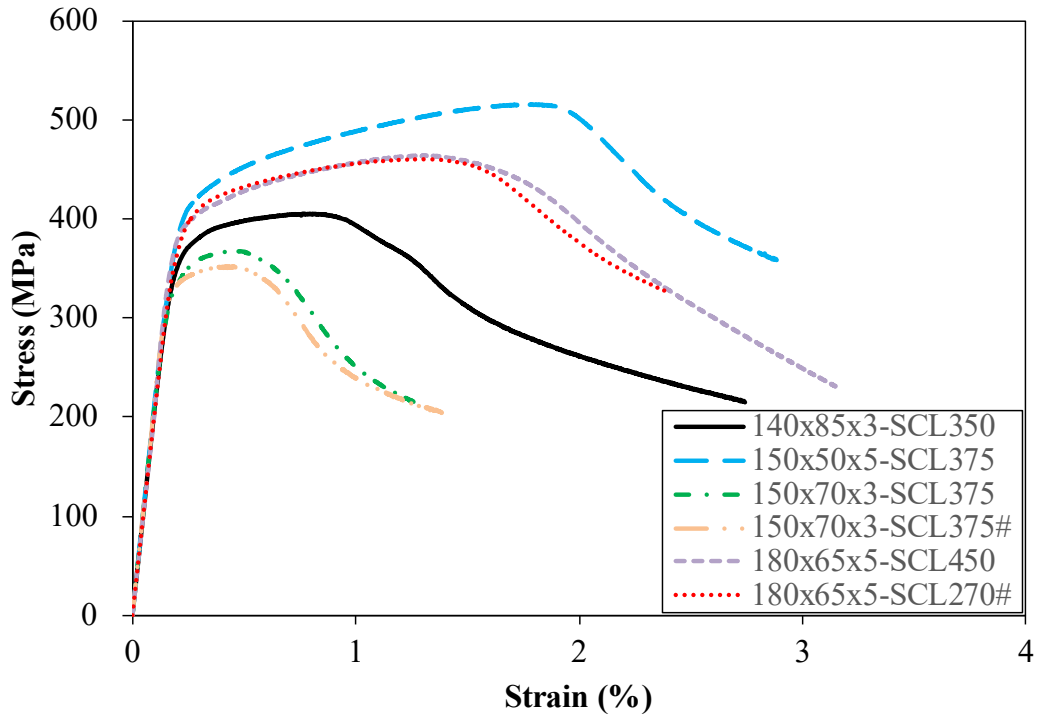


(a) Schematic view

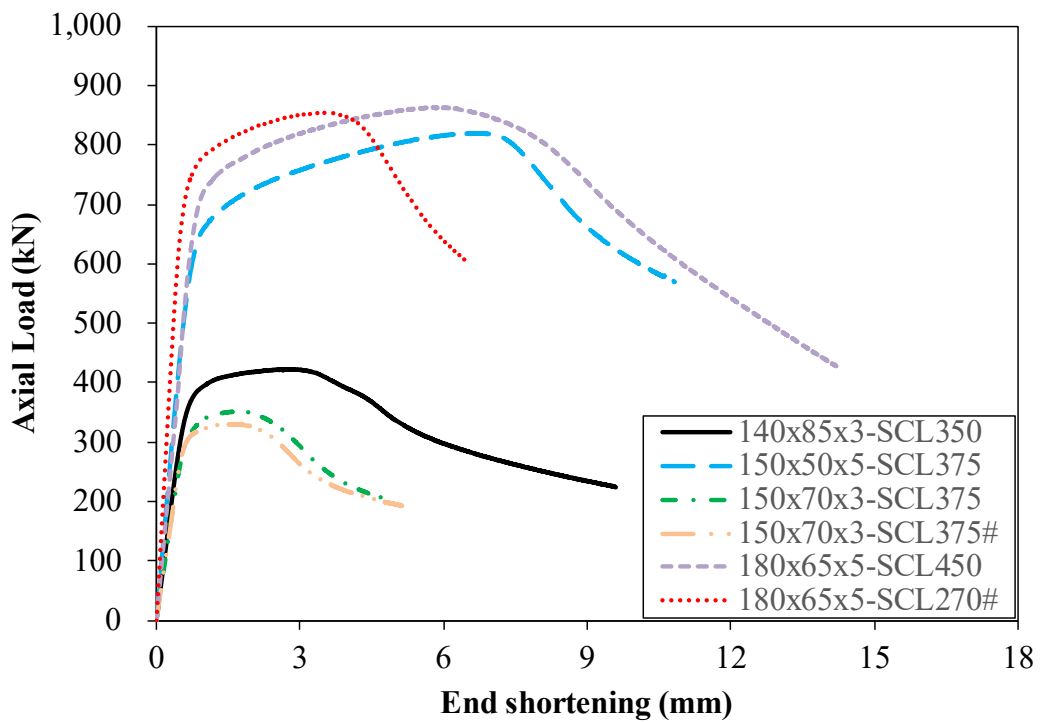


(b) Experimental arrangement

Figure 16. Setup of EHS stub column test



(a) Static stress-strain responses



(b) Static load-end shortening histories

Figure 17. Fixed-ended stub column test curves

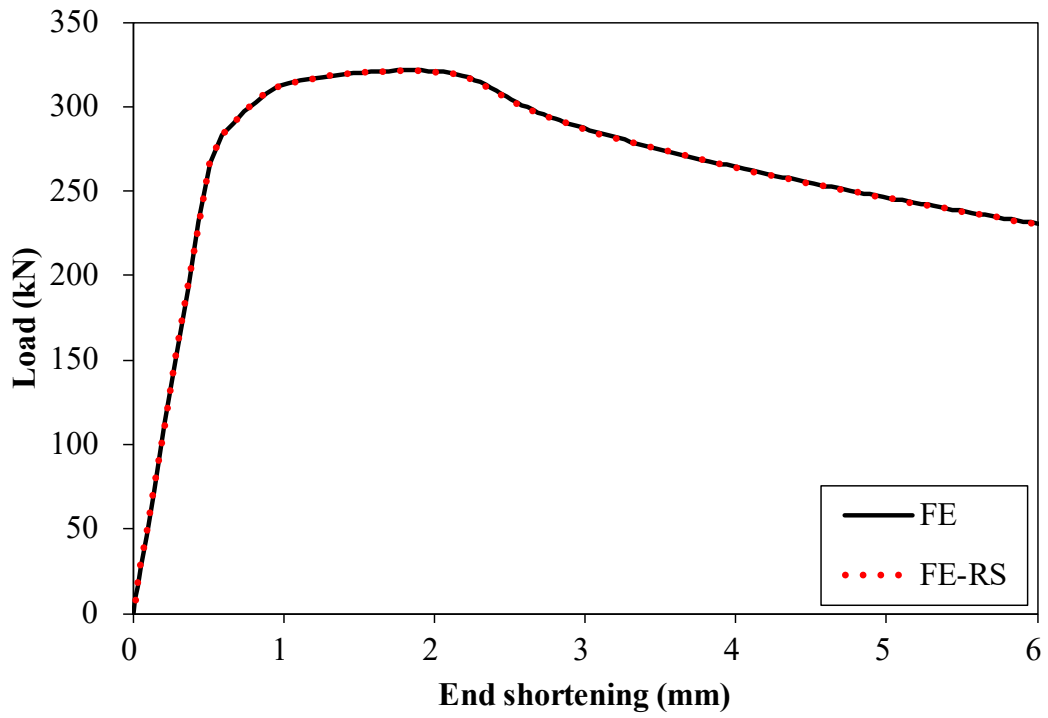


Figure 18. Comparison of FE models of EHS stub column 150×70×3-SCL375# with and without explicit inclusion of residual stress

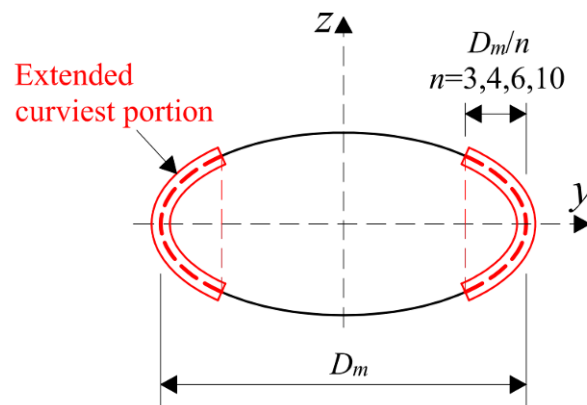


Figure 19. Extension of strength enhancement at the curviest portion of EHS

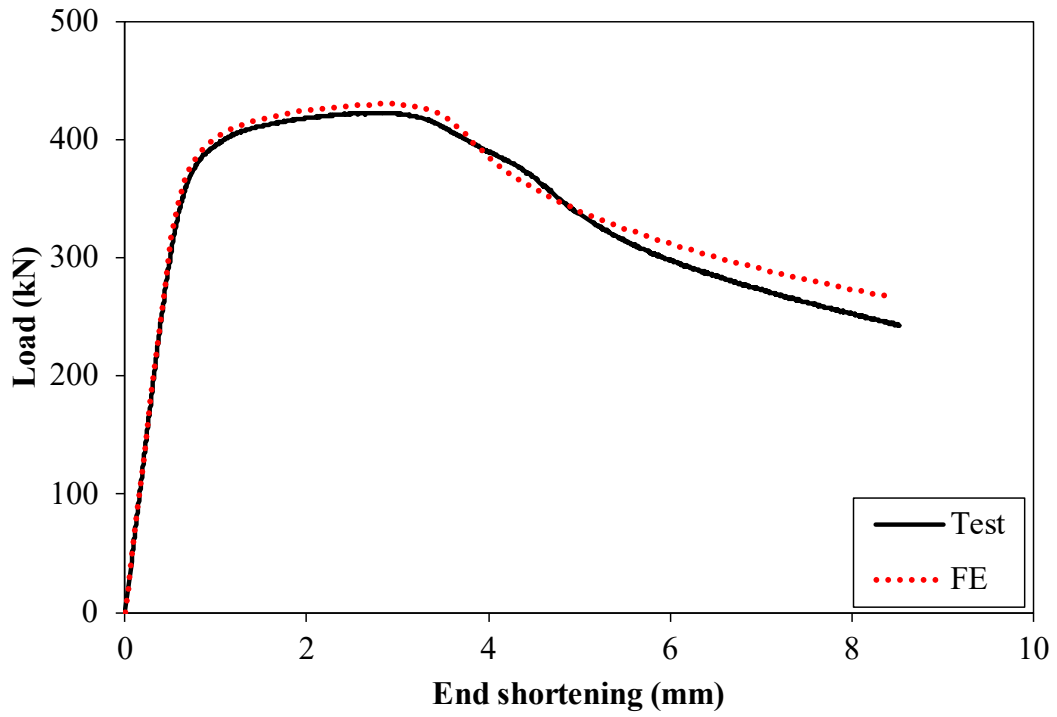


Figure 20. Experimental and numerical load-end shortening responses of EHS stub column
140×85×3-SCL350

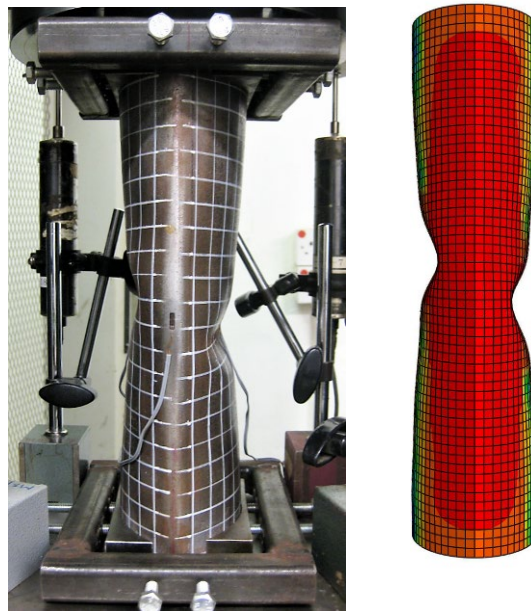


Figure 21. Comparison between experimental and numerical failure modes for EHS stub column
140×85×3-SCL350

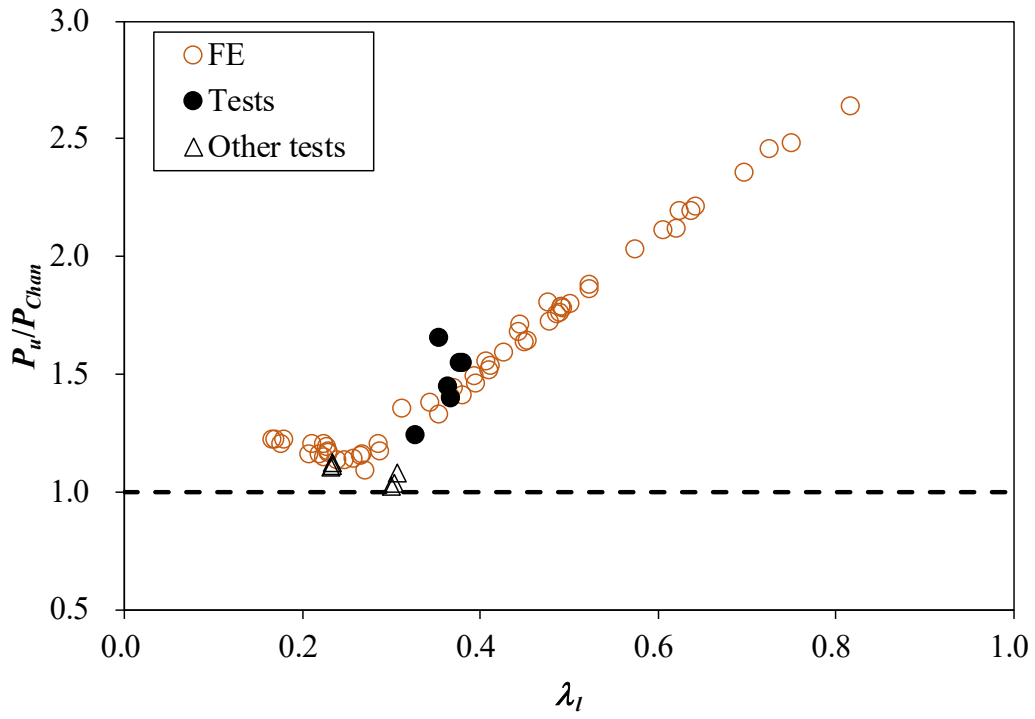


Figure 22. Comparison of test and FE results of EHS stub columns with design strengths predicted by the equivalent diameter method

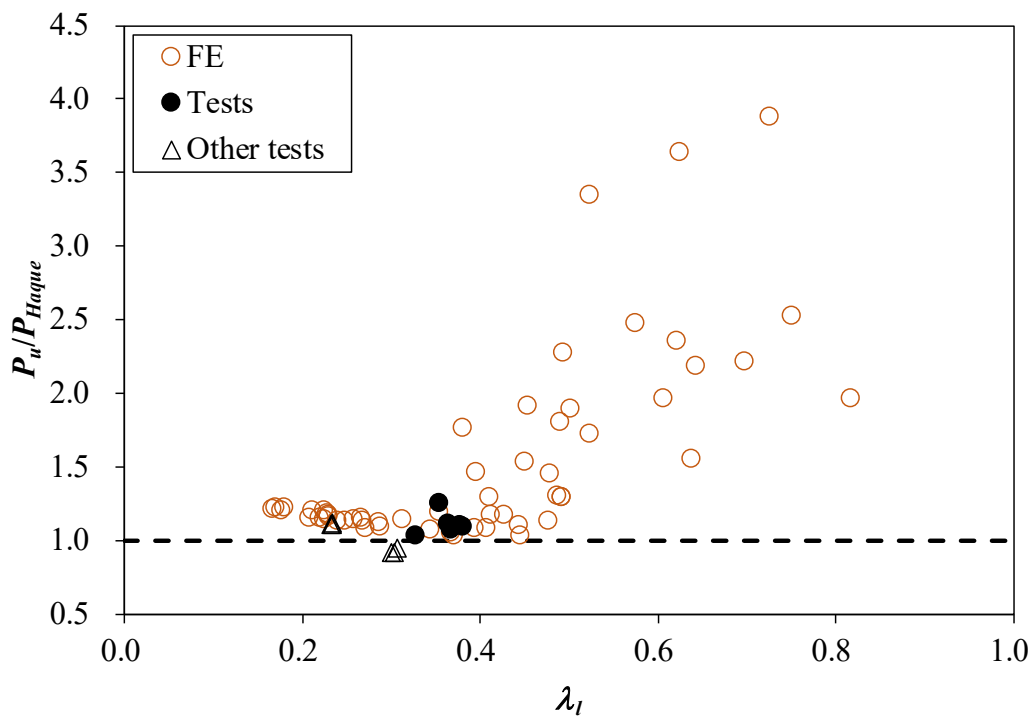


Figure 23. Comparison of test and FE results of EHS stub columns with design strengths predicted by the equivalent RHS approach

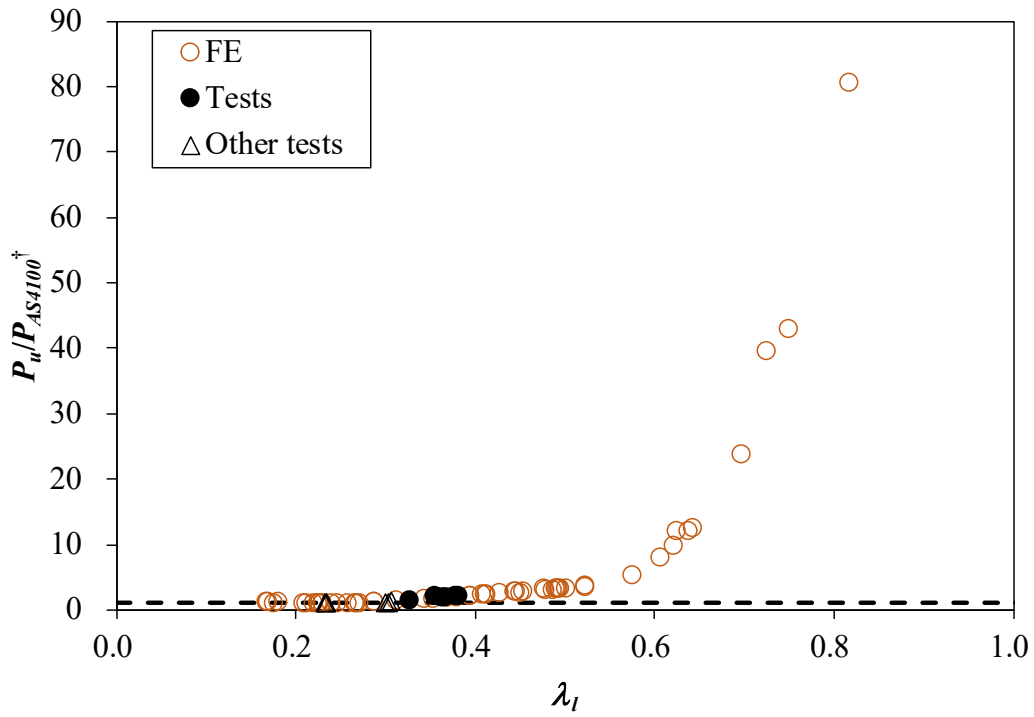


Figure 24. Comparison of test and FE results of EHS stub columns with design strengths predicted by the AS4100 [15] with equivalent diameter adopted

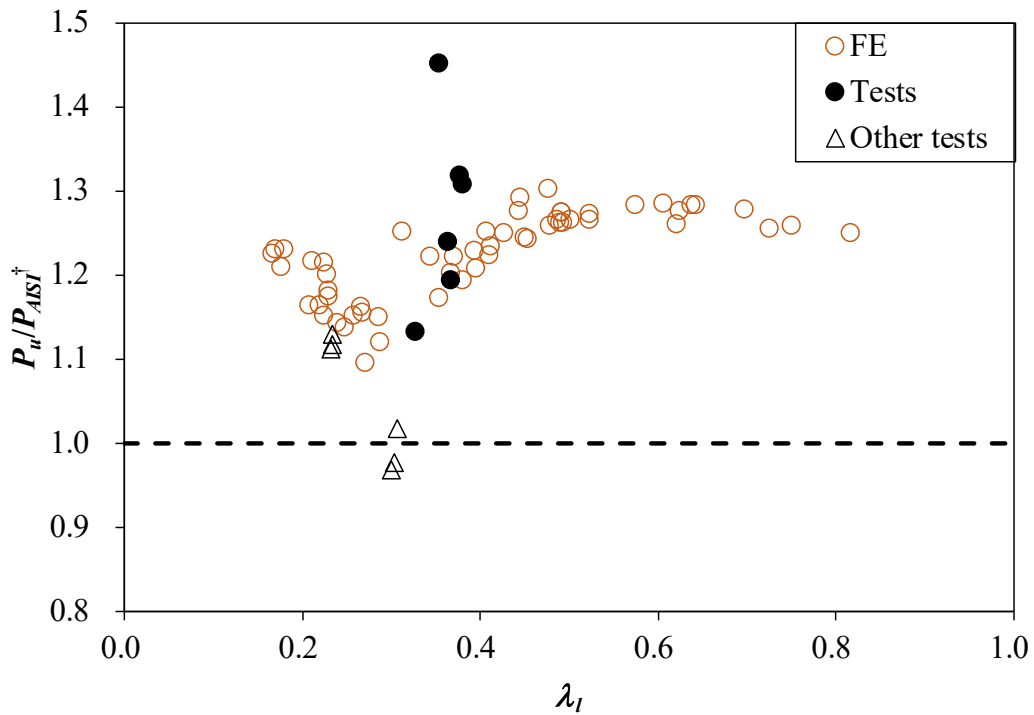


Figure 25. Comparison of test and FE results of EHS stub columns with design strengths predicted by the AISI-S100 [13] with equivalent diameter adopted

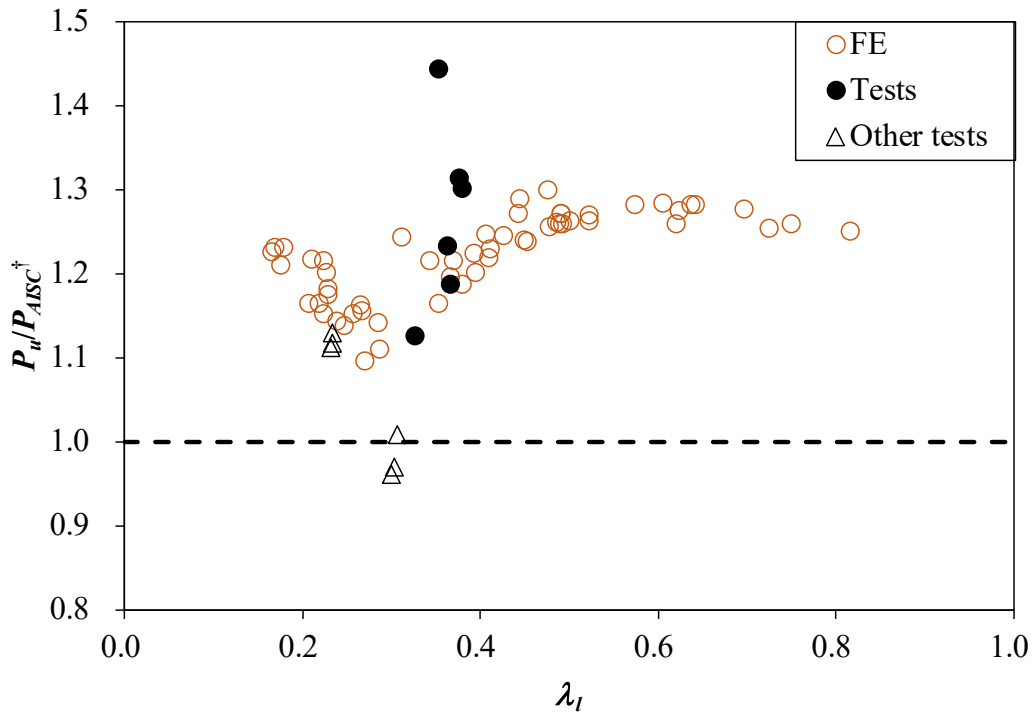


Figure 26. Comparison of test and FE results of EHS stub columns with design strengths predicted by the ANSI/AISC360 [14] with equivalent diameter adopted

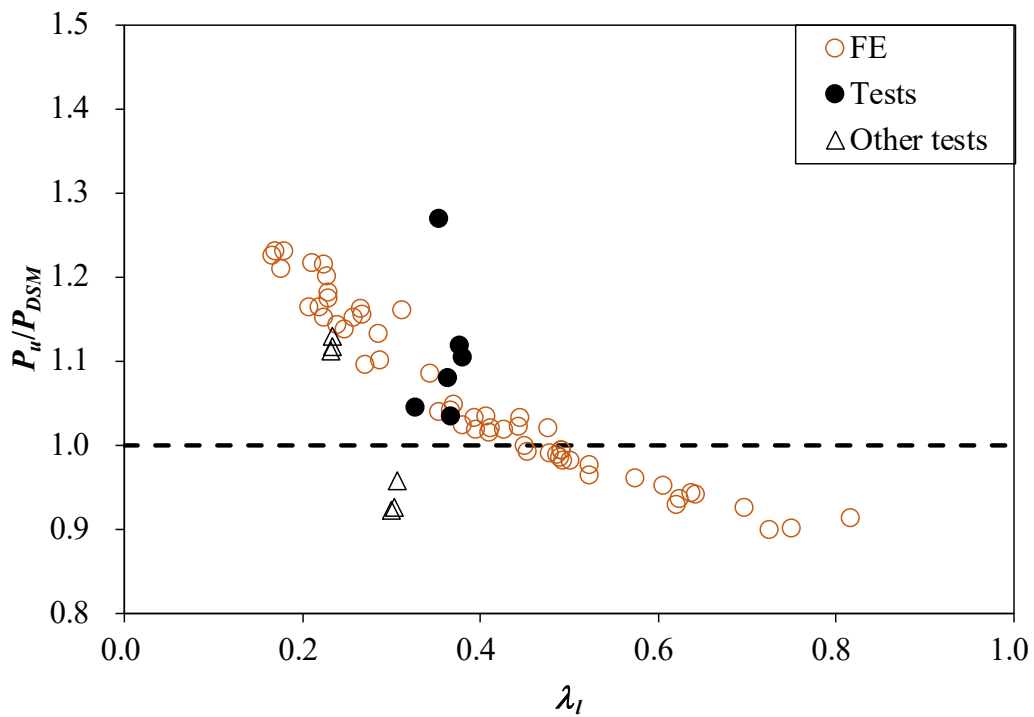


Figure 27. Comparison of test and FE results of EHS stub columns with design strengths predicted by the DSM

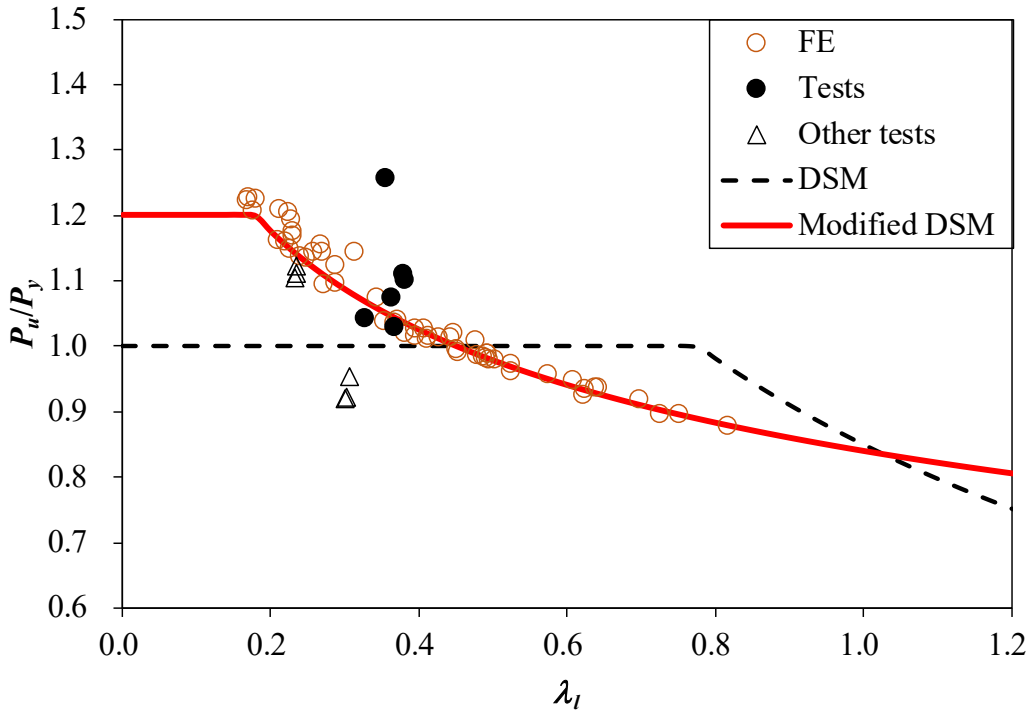


Figure 28. Comparison of test and FE results of EHS stub columns with design curves of the existing and modified DSM

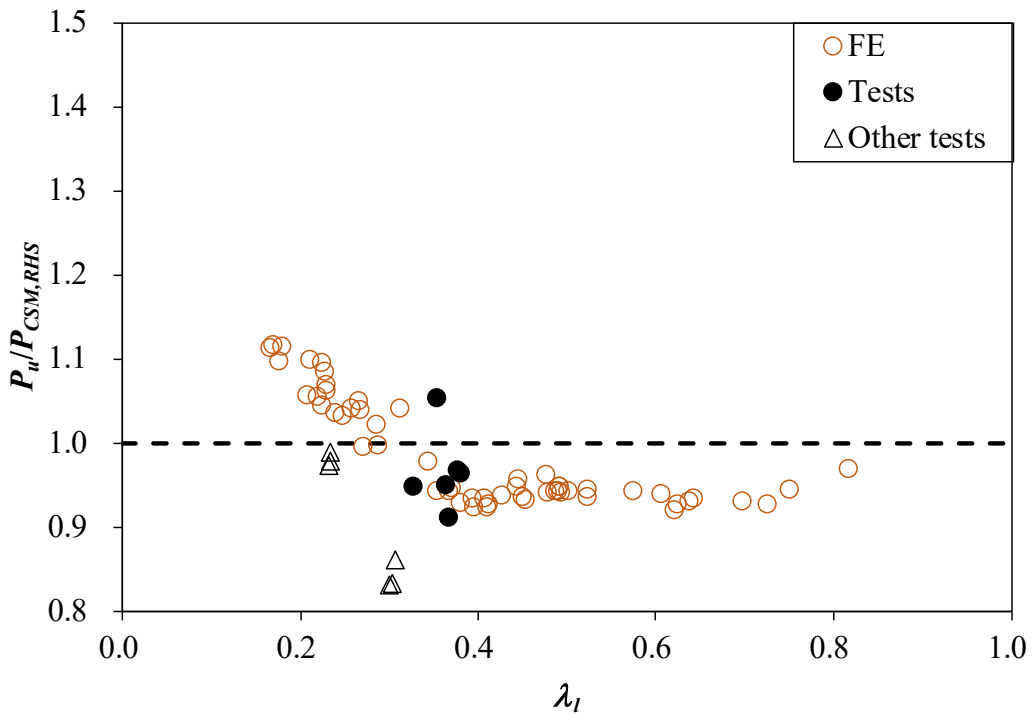


Figure 29. Comparison of test and FE results of EHS stub columns with design strengths predicted by the RHS approach of the CSM

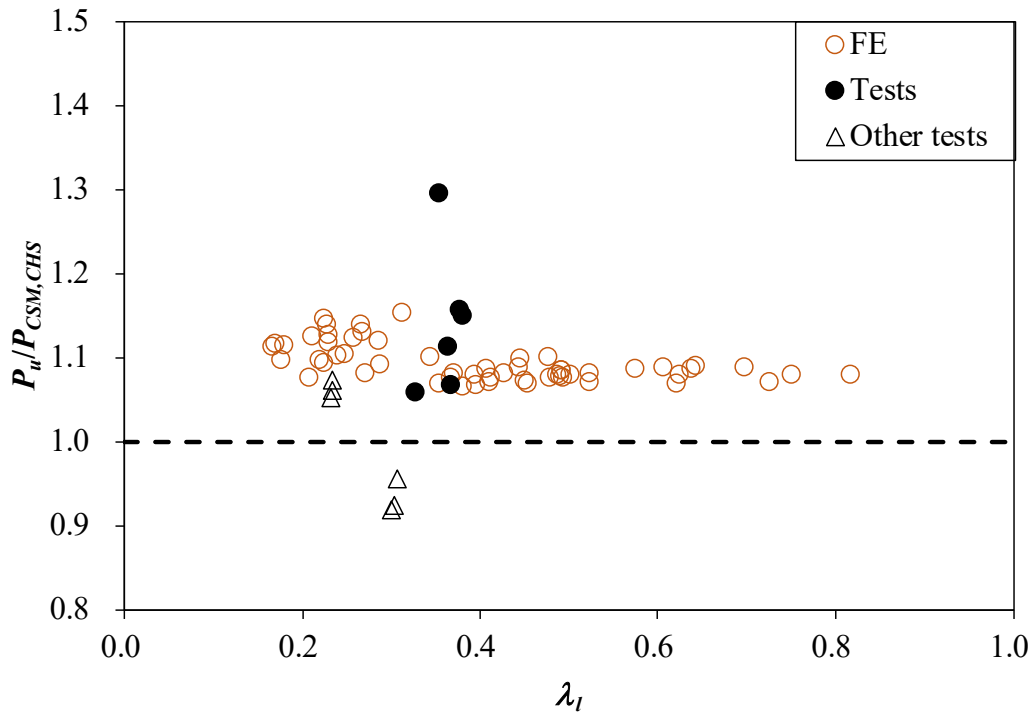


Figure 30. Comparison of test and FE results of EHS stub columns with design strengths predicted by the CHS approach of the CSM

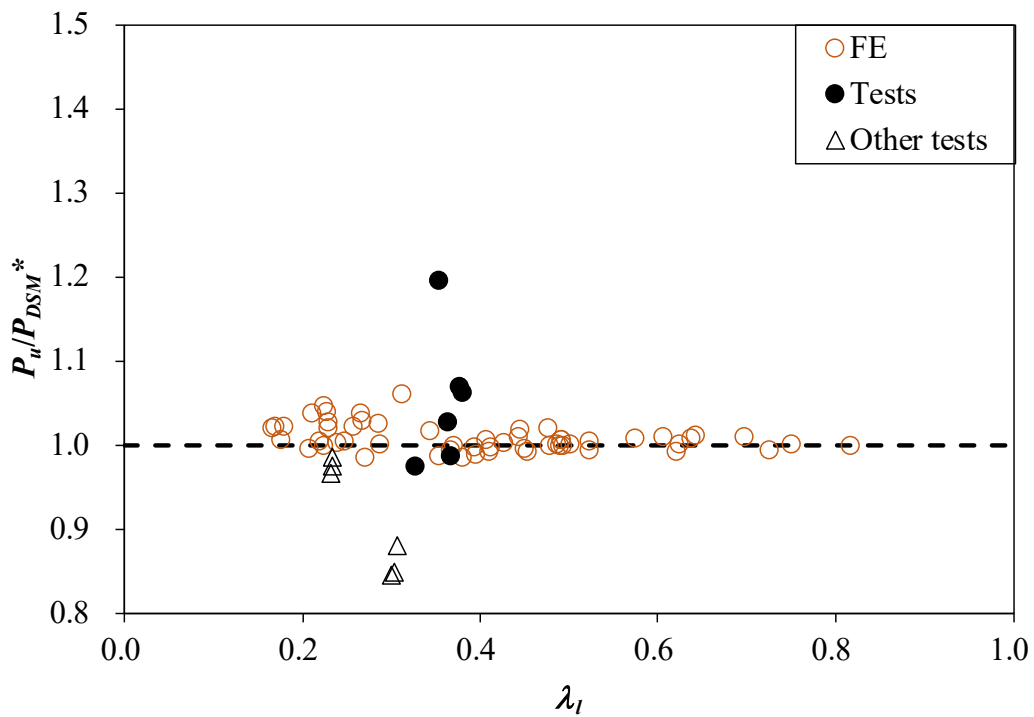


Figure 31. Comparison of test and FE results of EHS stub columns with design strengths predicted by the modified DSM

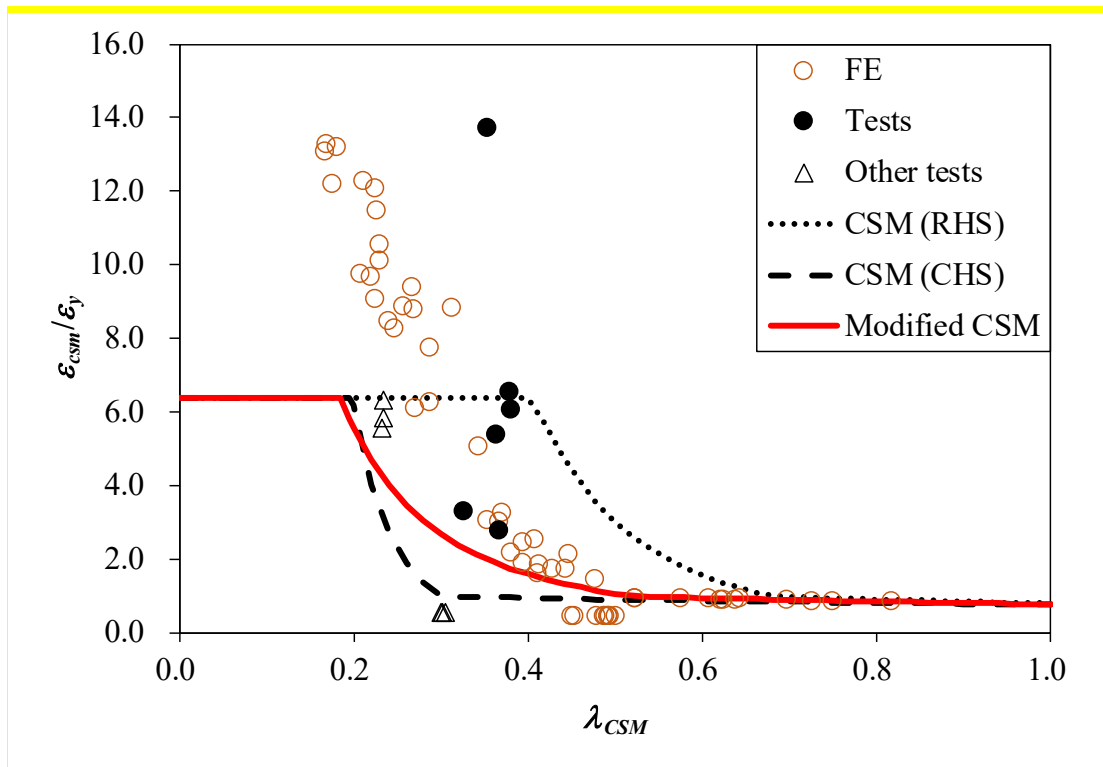


Figure 32. CSM base curves with experimental and numerical data

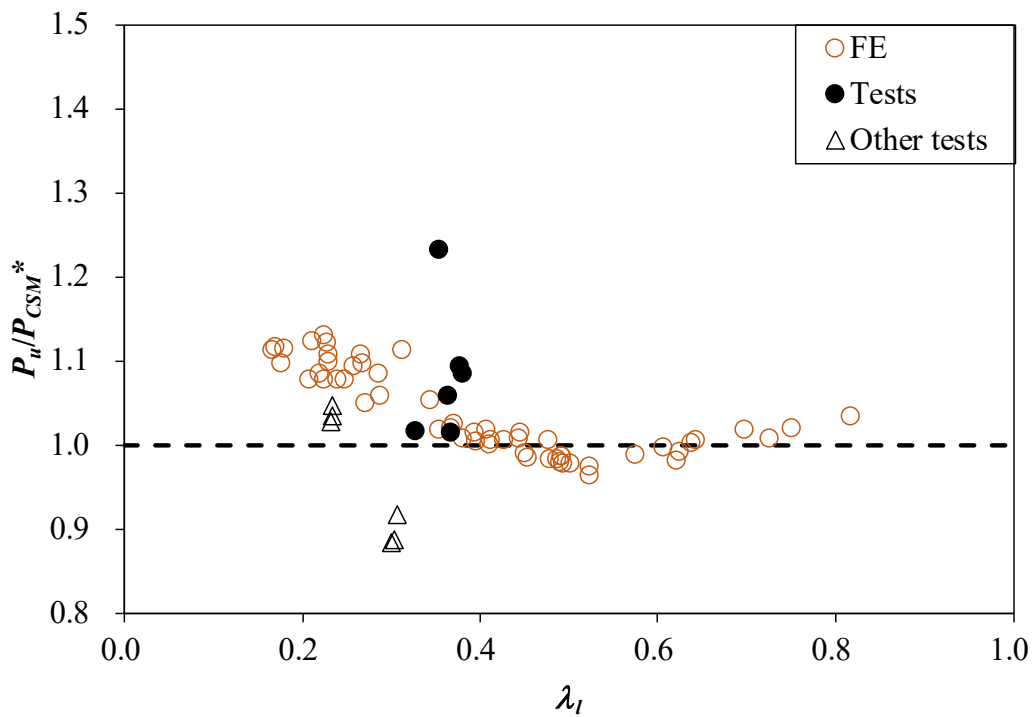


Figure 33. Comparison of test and FE results of EHS stub columns with design strengths predicted by the modified CSM

Section	Flattest Portion (TC1)				Curviest Portion (TC2)			
	E (GPa)	$\sigma_{0.2}$ (MPa)	σ_u (MPa)	ε_f (%)	E (GPa)	$\sigma_{0.2}$ (MPa)	σ_u (MPa)	ε_f (%)
140×85×3	208	388	433	14	213	401	458	13
150×50×5	205	410	521	20	213	529	654	12
150×70×3	210	341	392	16	210	340	397	14
180×65×5	200	418	499	19	206	533	635	12

Table 1. Measured material properties of EHS obtained from tensile coupon tests

Coupon location	E (GPa)	$\sigma_{0.2}$ (MPa)	σ_u (MPa)	ε_f (%)	Coupon location	E (GPa)	$\sigma_{0.2}$ (MPa)	σ_u (MPa)	ε_f (%)
1	212	380	414	16	15	215	344	410	16
2	217	508	538	11	16	206	353	409	15
3	211	427	450	13	17	216	377	432	16
4	215	385	422	15	18	205	404	445	13
5	212	383	418	15	19	211	385	434	14
6	216	395	433	14	20	211	388	432	14
7	215	373	419	16	21	215	381	425	15
8	209	386	426	14	22	210	382	425	14
9	211	379	439	13	23	218	383	423	18
10	201	392	435	14	24	212	388	428	14
11	209	373	431	13	25	214	359	412	16
12	201	359	414	15	26	210	371	417	15
13	211	363	415	15	27	211	356	412	16
14	211	380	429	13					

Table 2. Measured material properties obtained from tensile coupon tests in half-section of EHS

150×70×3

Specimen	D (mm)	B (mm)	t (mm)	ω_l	
				Convex (mm)	Concave (mm)
140×85×3-SCL350	141.2	87.2	2.94	0.591	-0.905
150×50×5-SCL375	150.4	51.1	4.95	0.263	-0.741
150×70×3-SCL375	148.7	71.6	2.75	0.530	-0.940
150×70×3-SCL375#	148.4	71.2	2.70	0.520	-1.114
180×65×5-SCL450	176.6	65.7	4.81	0.468	-1.579
180×65×5-SCL270#	176.8	64.8	4.81	-	-

Note: The local geometric imperfection of 180×65×5-SCL270# was not measured.

Table 3. Measured dimensions and local geometric imperfections of EHS stub columns

Specimen	E_{SC}	$\sigma_{0.2-SC}$	σ_{u-SC}	$\sigma_{0.2-TC}$	σ_{u-TC}
	(GPa)	(MPa)	(MPa)	$\sigma_{0.2-TC}$	σ_{u-TC}
140×85×3-SCL350	209	392	405	1.01	0.94
150×50×5-SCL375	217	441	515	1.08	0.99
150×70×3-SCL375	215	364	367	1.07	0.93
150×70×3-SCL375#	217	350	352	1.03	0.89
180×65×5-SCL450	208	418	464	1.00	0.93
180×65×5-SCL270#	207	424	460	1.02	0.92

Table 4. Cross-sectional material properties obtained from EHS stub column tests

Specimen	P_{Exp}	δ_u	P_y	$\frac{P_{Exp}}{P_y}$
	(kN)	(mm)	(kN)	
140×85×3-SCL350	422.5	2.8	405.2	1.04
150×50×5-SCL375	819.7	6.7	651.4	1.26
150×70×3-SCL375	351.8	1.7	325.5	1.08
150×70×3-SCL375#	330.5	1.6	319.1	1.04
180×65×5-SCL450	863.2	5.9	777.2	1.11
180×65×5-SCL270#	854.0	3.4	775.3	1.10

Table 5. EHS stub column test results

Specimen	P_{Exp}/P_{FE}				P_{Exp}/P_{FE}			
	Material division				Local imperfection			
	$D_m/3$	$D_m/4$	$D_m/6$	$D_m/10$	$t/3$	$t/10$	$t/50$	$t/100$
140×85×3-SCL350	0.95	0.96	0.97	0.98	1.13	1.03	0.98	0.97
150×50×5-SCL375	0.92	0.96	1.00	1.05	1.15	1.05	1.01	1.00
150×70×3-SCL375	1.05	1.05	1.06	1.06	1.22	1.11	1.07	1.07
150×70×3-SCL375#	1.01	1.01	1.02	1.02	1.17	1.06	1.03	1.02
180×65×5-SCL450	0.84	0.88	0.92	0.97	1.10	0.98	0.94	0.93
180×65×5-SCL270#	0.85	0.88	0.93	0.97	1.11	0.99	0.94	0.93
Mean	0.94	0.96	0.98	1.01	1.15	1.04	0.99	0.99
COV	0.090	0.073	0.053	0.040	0.038	0.048	0.053	0.054

Table 6. Summary of sensitivity study of EHS stub columns

Specimen	λ_d	P_{FE} (kN)	Specimen	λ_d	P_{FE} (kN)
500×250×25-SCL1250	0.23	12886.9	150×100×6-SCL375	0.22	1012.7
500×250×16-SCL1250	0.29	7929.0	150×100×2.5-SCL375	0.35	392.1
500×250×8-SCL1250	0.41	3748.2	150×75×8-SCL375	0.23	1239.8
500×200×20-SCL1250	0.29	9535.6	150×75×3-SCL375	0.37	428.1
500×200×12-SCL1250	0.37	5416.1	150×50×8-SCL375	0.27	1105.3
350×200×14-SCL875	0.24	5183.5	150×50×5-SCL375	0.34	667.4
350×200×5-SCL875	0.41	1699.5	150×50×3-SCL375	0.44	384.3
350×100×16-SCL875	0.31	5101.4	500×250×6-SCL1250	0.48	2743.0
350×100×8-SCL875	0.45	2346.5	500×250×3.5-SCL1250	0.62	1512.1
300×200×20-SCL750	0.17	6858.2	500×200×7-SCL1250	0.49	3036.5
300×200×10-SCL750	0.25	3360.1	500×200×3.5-SCL1250	0.70	1426.5
300×200×4-SCL750	0.39	1233.6	350×200×3.5-SCL875	0.49	1161.5
270×120×16-SCL675	0.23	4358.5	350×200×1.5-SCL875	0.72	457.6
270×120×4.5-SCL675	0.43	1102.3	350×100×7-SCL875	0.48	2036.5
250×200×20-SCL625	0.17	6147.7	350×100×2.5-SCL875	0.82	645.0
250×200×10-SCL625	0.21	3059.5	300×200×2.5-SCL750	0.49	747.5
250×200×6-SCL625	0.27	1761.1	300×200×1.5-SCL750	0.62	429.5
250×200×3-SCL625	0.38	833.3	270×120×3.5-SCL675	0.49	837.1
250×100×16-SCL625	0.22	3954.2	270×120×2-SCL675	0.64	458.6
250×100×12-SCL625	0.27	2906.4	250×200×1.5-SCL625	0.52	395.3
250×100×5-SCL625	0.41	1119.5	250×100×3.5-SCL625	0.49	759.1
210×120×16-SCL525	0.18	3649.5	250×100×1.5-SCL625	0.75	298.4
210×120×10-SCL525	0.22	2242.4	210×120×2-SCL525	0.50	397.1
210×120×2.5-SCL525	0.45	503.4	210×120×1.5-SCL525	0.57	292.3
180×80×12-SCL450	0.21	2184.8	180×80×1.5-SCL450	0.61	231.7
180×80×8-SCL450	0.26	1422.8	150×100×1.5-SCL375	0.45	226.4
180×80×3.5-SCL450	0.39	576.9	150×75×1.5-SCL375	0.52	203.4
150×100×12-SCL375	0.17	2056.2	150×50×1.5-SCL375	0.64	179.9

Table 7. Parametric study on cold-formed steel EHS stub columns

Number of		$\frac{P_u}{P_{Chan}}$	$\frac{P_u}{P_{Haque}}$	$\frac{P_u}{P_{AS4100}^\dagger}$	$\frac{P_u}{P_{AISI}^\dagger}$	$\frac{P_u}{P_{AISC}^\dagger}$	$\frac{P_u}{P_{DSM}}$	$\frac{P_u}{P_{CSM,RHS}}$	$\frac{P_u}{P_{CSM,CHS}}$	$\frac{P_u}{P_{DSM}^*}$	$\frac{P_u}{P_{CSM}^*}$
Test:12 [^]	FE:56										
ALL: 68	Mean	1.53	1.45	5.31	1.21	1.21	1.06	0.98	1.09	1.00	1.04
	COV	0.263	0.425	2.240	0.065	0.065	0.093	0.068	0.045	0.044	0.059
	ϕ	1.00	1.00	0.90	0.85	0.90	0.85	1.00	1.00	0.85	1.00
	β	2.50	1.72	0.97	3.53	3.29	2.87	1.83	2.32	2.82	2.08
	ϕ^Δ	0.85	0.85	0.85	0.85	0.85	0.85	0.85	0.85	0.85	0.85
	β^Δ	2.96	2.04	0.99	3.53	3.52	2.87	2.48	2.99	2.82	2.74

[^]: Test results from Chan *et al.* [25] are also included

[†]: Nominal design strengths predicted by adopting the equivalent diameter proposed by Chan *et al.* [11]

*: Modified design method

Δ : Reliability analysis with resistance factor of 0.85

Table 8. Comparison of EHS stub column test and FE results with predicted strengths